Elementary models with probability distribution function intermittency for passive scalars with a mean gradient

A. Bourlioux[a)]
Département de Math. et Stat., Université de Montréal, Montréal, Québec H3C 3J7, Canada

A. J. Majda
Courant Institute of Mathematical Sciences, New York, New York 10012

(Received 12 June 2001; accepted 7 November 2001)

The single-point probability distribution function (PDF) for a passive scalar with an imposed mean gradient is studied here. Elementary models are introduced involving advection diffusion of a passive scalar by a velocity field consisting of a deterministic or random shear flow with a transverse time-periodic transverse sweep. Despite the simplicity of these models, the PDFs exhibit scalar intermittency, i.e., a transition from a Gaussian PDF to a broader than Gaussian PDF with large variance as the Péclet number increases with a universal self-similar shape that is determined analytically by explicit formulas. The intermittent PDFs resemble those that have been found recently in numerical simulations of much more complex models. The examples presented here unambiguously demonstrate that neither velocity fields inducing chaotic particle trajectories with positive Lyapunov exponents nor strongly turbulent velocity fields are needed to produce scalar intermittency with an imposed mean gradient. The passive scalar PDFs in these models are given through exact solutions that are processed in a transparent fashion via elementary stationary phase asymptotics and numerical quadrature of one-dimensional formulas. © *2002 American Institute of Physics.* [DOI: 10.1063/1.1430736]

I. INTRODUCTION

Many practical applications in environmental science and engineering involve the behavior of a passive scalar with a mean gradient that is diffused and advected by a velocity field at high Péclet numbers. The single-point probability distribution (PDF) of a passive scalar has been the focus of much interest since the Chicago experiments in Rayleigh–Bénard convection.[1,2] They established that the PDF for the temperature at the center of a convection cell undergoes a transition from Gaussian behavior to a probability distribution with approximate exponential tails over a wide range of its variability as the underlying fluid flow becomes sufficiently turbulent. Such broader than Gaussian distributions for the scalar PDF with long tails exhibit the phenomena called passive scalar intermittency. These results have inspired a large research effort devoted to studying scalar intermittency for passive scalars with an imposed mean gradient through laboratory experiments,[3–6] phenomenological models,[7–11] and numerical experiments.[12–15] The phenomenological models[7–11] yield either Gaussian or exponential PDFs and require sufficiently turbulent flow fields with chaotic particle trajectories with positive Lyapunov exponents. The numerical experiments[12,13] yield a much wider class of PDFs with scalar intermittency with even broader tails than exponential in some regimes. In this context, the following questions naturally emerge. What structure is needed for a velocity field so that the PDF for a passive scalar in a mean gradient exhibits a transition from a Gaussian (or even sub-Gaussian) PDF at low Péclet numbers to a broader than Gaussian shape as the Péclet number increases? How universal is the shape of the PDF as the Péclet number gets arbitrarily large? In particular, are the following structural conditions on the velocity field needed for passive scalar intermittency:

(a) Velocity fields with chaotic particle trajectories and at least one positive Lyapunov exponent?

(b) Many turbulent scales in the velocity field?

(c) Statistical random fluctuations of at least one scale in the velocity field?

Our goal in the present paper is to introduce and analyze a simple class of models where all of the above questions can be answered in a precise unambiguous fashion. The models studied here involve passive scalar advection–diffusion in the nondimensional form

$$\frac{\partial T}{\partial t} + \mathrm{Pe}(\mathbf{v}\cdot\nabla T) = \Delta T. \tag{1}$$

These models utilize the special incompressible two-dimensional velocity fields given by a time-dependent shear flow with a transverse sweep, i.e.,

$$\mathbf{v} = (v(y,t), w(t)), \tag{2}$$

where $v(y,t)$ is deterministic or random and

$$w(t) = w_0 + \beta \sin(\omega t) \tag{3}$$

[a)]Electronic mail: Anne.Bourlioux@UMontreal.ca

is a periodic function of time of period $\tau_P = 2\pi/\omega$ and of constant mean w_0. The PDF for the scalar in the model with (1), (2) is treated in the statistically stationary state with a mean gradient along the x axis, i.e.,

$$T = \frac{x}{L_g} + T'(x,y,t). \tag{4}$$

The nondimensonalization used in (1) is completely standard with spatial units chosen by the largest length scale L of the velocity field and the Péclet number given by $\mathrm{Pe} = VL/\kappa$, where V is the typical magnitude of v with w assumed to have comparable magnitude while κ is the diffusivity of the scalar. The quantity L_g^{-1} in (4) measures the magnitude of the imposed scalar gradient in these nondimensional units.

The passive scalar PDFs in these models are given through exact solutions that are processed below via elementary stationary phase asymptotics and numerical quadrature of one-dimensional formulas. Despite the simplicity of the models in (1), (2), (4) the PDF for the scalar exhibits PDF intermittency as the Péclet number increases, provided, for example, the velocity field $v(y,t)$ is nonzero and the periodic transverse sweep $w(t)$ has isolated zeros. The universal limiting broad-tail shape is determined analytically through explicit formulas. As a preview of the results developed below, Figs. 2 and 4 explicitly display scalar intermittency with a universal limiting shape as $\mathrm{Pe} \to \infty$ for the deterministic steady single spatial mode shear flow with a purely sinusoidal transverse sweep:

$$v(y,t) = \sin(2\pi y), \quad w(t) = \sin(\omega t), \tag{5}$$

while Figs. 5 and 6 below show scalar intermittency for the PDFs with a steady single mode shear with Gaussian random amplitude and the same transverse sweep from (5). The broad tail PDFs in these figures strongly resemble those found in Fig. 1 from Ref. 12 and Fig. 6, Fig. 16, and Fig. 19 from Ref. 13, which were post-processed from numerical simulations of much more complex models. These examples demonstrate unambiguously that surprisingly, none of the detailed structural conditions (a), (b), (c) above for the velocity field are needed to get very strong passive scalar intermittency with a prescribed mean gradient. What is the source of intermittency in the elementary models with the velocity field in (2)? When $w(t)$ has an isolated zero in time, the streamline topology for the flow field changes from completely blocked behavior in the x direction parallel to the imposed mean scalar gradient to very rapid transport in the x direction for a small interval of time around the zero of $w(t)$. This change of topology is illustrated in Fig. 1: when $w = 0$, the open streamlines in the horizontal direction, along the mean gradient, lead to large convective transport and large deformations of the isocontours for the scalar, which promote strong mixing by diffusion. When $w \neq 0$, however, the transverse sweep corresponds to blocked streamlines, little transport along the gradient, weak distortion of the scalar isocontours, and, hence, ultimately, little opportunity for mixing by diffusion. With the time-modulated transverse sweep used in this paper, blocked streamlines are observed most of the time, except for the rare occasions when the transverse sweep is zero, which leads to bursts of strong

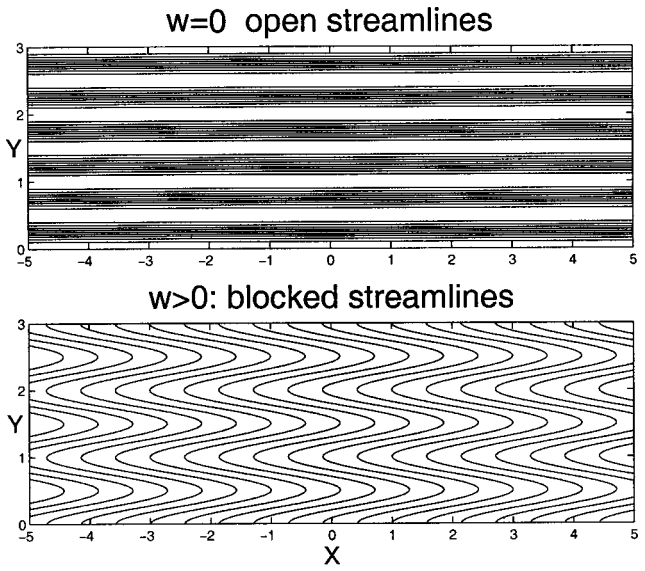

FIG. 1. Effect of the transverse sweep on the topology of the streamlines.

mixing; this on/off mechanism that controls turbulent mixing via streamlines blocking and opening defines what is meant by intermittency in the present setup by reference to qualitatively similar phenomena in more complex systems. This intuitive reasoning is made more precise in the detailed analysis below and already played a similar role in previous work of Kramer and the second author,[16] where scaling laws for the turbulent diffusivity of the models in (1), (2) were calculated asymptotically at high Péclet numbers. The philosophy of the work presented here to develop explicit models with unambiguous behavior for intermittency of scalar PDFs has also been utilized for decaying passive scalars at long times[16–18] with recent powerful results demonstrating families of stretched exponential tails in the long time limit.[19–21]

The organization of the remaining parts of the paper is as follows. Section II has exact solution formulas for the model in (1), (2), (4) as well as an important collection of elementary formulas for scalar PDFs for the model. The behavior of the turbulent diffusivity for the model in (1), (2), (4) at finite large Péclet numbers is studied in Sec. III in order to link the behavior of large variance in the passive scalar statistics with the intermittency scenario in the geometry of streamlines transverse to the mean gradient mentioned earlier; this provides important intuition and a link with subsequent results on scalar intermittency. Also, the high Péclet number scaling analysis[16] is confirmed. The results briefly discussed above for the special case of a steady single mode shear are developed in Sec. IV. The situation where the velocity field $v(y,t)$ is a Gaussian random field in space–time with a finite correlation time is developed in Sec. V; scalar intermittency in this case is more subtle because the scalar PDF for the model in (1), (2), (4) in the extreme limiting case with δ correlation in time in the velocity field $v(y,t)$ is Gaussian for all (even arbitrarily large) Péclet numbers.

II. BASIC FORMULAS FOR THE MODEL

With the model in (1), (2), (4), the first important fact to realize is that in the statistically stationary state, T' from (4) can be chosen as a function of y and t alone so that T' satisfies the linear equation:

$$\frac{\partial T'}{\partial t}+\mathrm{Pe}\, w(t)\frac{\partial T'}{\partial y}-\frac{\partial^2 T'}{\partial y^2}=-\frac{\mathrm{Pe}}{L_g}v(y,t). \tag{6}$$

Of course, in order to be a valid statistically stationary state, T' needs to have zero mean over the ensemble average:

$$\langle T'(y,t)\rangle=0, \tag{7}$$

where $\langle\cdot\rangle$ denotes the ensemble average over the probability space associated with the shear velocity statistics for $w(t)$ and $v(y,t)$. Here, the transverse sweep $w(t)$ is always chosen as a periodic function of time with period τ_P so that the appropriate average over the velocity statistics for w is the time average over a period,[22]

$$\langle F\rangle_{\tau_P}=\frac{1}{\tau_P}\int_t^{t+\tau_P}F(\tau)d\tau, \tag{8}$$

where the random variable $F(\tau)$ is tacitly assumed to be a periodic function of τ that might also depend on other parameters. In this paper, the shear velocity field $v(y,t)$ will have a variety of statistics in different scenarios ranging from a deterministic steady velocity to a general spatiotemporal Gaussian random field.[23] The average over the probability space associated with the shear velocity statistics is denoted by $\langle\cdot\rangle_v$ and it is always assumed for simplicity that the velocity v has zero mean, i.e., $\langle v\rangle_v=0$. By combining this information with (8), the average $\langle\cdot\rangle$ over the probability space associated with the velocity statistics $w(t)$, $v(y,t)$ of a random variable $F(\tau,\cdot)$ is given by the iterated average:

$$\langle F\rangle=\langle\langle F\rangle_v\rangle_{\tau_P}, \tag{9}$$

and this yields the concrete form of the important requirement in (7) for the statistical stationarity of T'.

To build the solution of (6) satisfying the statistically stationary requirement in (7), assume that $v(y,t)$ has the expansion in spatial modes with wave numbers $K_J\neq 0$,

$$\begin{aligned} &v(y,t)=\sum_J \hat{v}_J e^{iK_J y},\\ &\overline{\hat{v}_J(t)}=\hat{v}_{-J}(t), \quad \text{reality condition}, \end{aligned} \tag{10}$$

where the amplitudes $\hat{v}_J(t)$ are statistically stationary complex Gaussian random fields in time in the most general case.[23] Seek the statistically stationary solution $T'(y,t)$ through the related expansion:

$$T'(y,t)=\frac{\mathrm{Pe}}{L_g}\sum_J \widehat{T'_J}e^{iK_J y}, \quad \text{with} \quad \overline{\widehat{T'_J}}(t)=\widehat{T'}_{-J}, \tag{11}$$

where, by substitution in (6), $\widehat{T'_J}$ satisfies the following linear inhomogeneous ODEs:

$$\frac{d\widehat{T'_J}}{dt}+[K_J^2+iK_J\,\mathrm{Pe}\, w(t)]\widehat{T'_J}=-\hat{v}_J. \tag{12}$$

The solution for $\widehat{T'_J}$ is readily obtained via Duhamel's formula to yield the following explicit formula for the stationary solution to (6), (7), (12):

$$T'(y,t)=\frac{\mathrm{Pe}}{L_g}\sum_J \widehat{T'_J}(t)e^{iK_J y},$$

with

$$\widehat{T'_J}(t)=-\int_{-\infty}^{t}S_{K_J}(t,t')\hat{v}_J(t')dt', \tag{13}$$

where S_{K_J} is the explicit solution operator:

$$S_{K_J}(t,t')=e^{-K_J^2(t-t')}e^{-iK_J\,\mathrm{Pe}\int_{t'}^{t}w(s)ds}. \tag{14}$$

Note that it is crucial that the integral in (13) begins at $-\infty$ in order to guarantee statistical stationarity; furthermore, for the random amplitudes $\hat{v}_J(t')$ utilized in this paper that are either steady of time-dependent complex Gaussian random variables with rapidly decaying correlations, the integral in (13) converges for almost every realization because $S_{K_J}(t,t')$ has the exponential damping term $e^{-K_J^2(t-t')}$ for $t'<t$.

A. Formulas for the PDF of *T*

The PDF of a random variable Z defined on the probability space of the velocity statistics is by definition[23] the positive density $p_Z(\lambda)$ with $\int p_Z(\lambda)d\lambda=1$, so that

$$\int_{-\infty}^{\infty}\phi(\lambda)p_Z(\lambda)d\lambda=\langle\phi(Z)\rangle, \tag{15}$$

for all bounded continuous functions ϕ. In the applications below for calculating the PDF of T, the partial PDF of T obtained by averaging over the shear velocity statistics will be known explicitly as a periodic function of t with period τ_P. Thus, assume that

$$\text{the partial PDF } p_{Z(t)} \text{ is a given periodic function of } t \text{ with period } \tau_P. \tag{16}$$

Then, with the formulas in (15) and (8), it is easy to show that the complete PDF for Z is given by the time average

$$p_Z=\frac{1}{\tau_P}\int_0^{\tau_P}p_{Z(t)}dt. \tag{17}$$

Next, the formulas in (16), (17) will be applied to the PDF for T for several different cases developed below. Clearly, the imposed deterministic mean gradient for T in (4) creates only a trivial shift in the PDF of T' so only the PDF of T' will be calculated throughout the remainder of the paper.

B. A deterministic steady single mode shear

For a deterministic single mode shear,

$$v(y)=\sin(2\pi y), \tag{18}$$

the stationary solution $T'(y,t)$ is given by

$$T'(y,t)=\sigma(t)\sin[2\pi y+\theta(t)], \tag{19}$$

where $\sigma^2(t)$, $\theta(t)$, respectively, are an explicit time periodic amplitude and phase shift with detailed formulas presented in Secs. III, IV. For shear velocity fields that are deterministic and spatially periodic with period 1, the average over the shear velocity statistics is the periodic average,[22] $\langle F\rangle_v = \int_0^1 F(y)dy$. With this fact and the definition in (15), it is easy to show by changing variables that the explicit PDF of $Z=\sigma\sin(2\pi y+\theta)$ with $\sigma>0$ is given by

$$p_Z(\lambda)=\frac{1}{\sigma}P_0\left(\frac{\lambda}{\sigma}\right), \tag{20}$$

with

$$P_0(\lambda)=\frac{1}{\pi}\begin{cases}(1-\lambda^2)^{-1/2}, & \text{when}|\lambda|<1,\\ 0, & \text{when}|\lambda|\geqslant 1.\end{cases}$$

With the facts in (16), (17), (19), and (20), the PDF of $T'(y,t)$ can be calculated in this case through the formula

$$p_{T'}(\lambda)=\frac{1}{\tau_P}\int_0^{\tau_P}\frac{1}{\sigma(t)}P_0\left(\frac{\lambda}{\sigma(t)}\right)dt, \tag{21}$$

which is utilized in Sec. IV below.

C. Stationary Gaussian random shear flows

Assume that the velocity field $v(y,t)$ is a stationary Gaussian random field so that the wave amplitudes for v from (10) are stationary Gaussian random fields. Then the formulas in (13), (14) guarantee that $T'(y,t)$, a superposition of Gaussian random variables, is also a Gaussian random variable that has mean zero and that is stationary in y for each fixed time t. Thus, the partial PDF, $p_{T'(t)}$, is Gaussian independent of y and given explicitly by the formula

$$\begin{aligned}&p_{T'(t)}(\lambda)=\frac{1}{\sqrt{2\pi}\sigma(t)}e^{-\lambda^2/2\sigma^2(t)}=\frac{1}{\sigma(t)}G\left(\frac{\lambda}{\sigma(t)}\right),\\ &\sigma^2(t)=\langle|T'(t)|^2\rangle_v,\end{aligned} \tag{22}$$

with $G(\lambda)=(2\pi)^{-1/2}\exp(-\lambda^2/2)$ the normalized Gaussian. The partial scalar variance $\sigma^2(t)$ is an explicit periodic function of time that is readily calculated through the formulas in (13) and (14) (see Secs. IV, V). In this situation, the complete PDF of T' is determined through (17) and (22) by

$$p_{T'}(\lambda)=\frac{1}{\tau_P}\int_0^{\tau_P}\frac{1}{\sigma(t)}G\left(\frac{\lambda}{\sigma(t)}\right)dt. \tag{23}$$

We will assume that the random Fourier amplitudes in $\hat{v}_J(t)$ have the form[23]

$$\begin{aligned}&\hat{v}_J(t)=\tfrac{1}{2}[\,\eta_J(t)-i\xi_J(t)], \quad J>0,\\ &\hat{v}_{-J}(t)=\tfrac{1}{2}[\,\eta_J(t)+i\xi_J(t)],\end{aligned} \tag{24}$$

where $\eta_J(t)$ and $\xi_J(t)$ are real Gaussian random fields that are independent and also independent for $J\neq J'$ with covariance $R_J(|t|)$ given by

$$\langle\,\eta_J(t+t_0)\,\eta_J(t_0)\rangle_v=\langle\xi_J(t+t_0)\xi_J(t_0)\rangle_v=R_J(|t|). \tag{25}$$

The steady case studied in Sec. IV is the formal extreme limiting case with $R_J(|t|)=R_J(0)$. Note that $R_J(0)\equiv E_J$ is the energy in the Jth mode. Under these assumptions, the scalar variance $\sigma^2(t)$ is given by

$$\sigma^2(t)=2\,\frac{\mathrm{Pe}^2}{L_g^2}\sum_J\,\langle|\widehat{T'_J}(t)|^2\rangle_v, \tag{26}$$

with $\widehat{T'_J}$ determined by (13).

We conclude this section with the following remark. Clearly, with the concrete formulas in (21) and (23) the issues regarding passive scalar intermittency in the model defined in (1), (2), (4) reduce to finding bursting time intervals of the basic period τ_P, where on these intervals the scalar variance satisfies $\sigma^2(t)\gg\langle\sigma^2\rangle_{\tau_P}$. In the next sections, we establish that this is the situation as the Péclet number increases, provided that the transverse sweep $w(t)$ in the model has isolated zeros.

III. TURBULENT DIFFUSIVITY IN THE MODEL

In this section, explicit expressions are presented for the turbulent diffusivity resulting from a deterministic steady single mode shear $v(y)=\sin(2\pi y)$ (as in Sec. II B). Our objective in this section is to illustrate via an extremely simple example the mechanism by which isolated zeros in the transverse sweep can lead to bursts of activity and an interesting intermittent passive scalar response. The turbulent diffusivity κ_T can be computed directly according to the following formula:[16]

$$\kappa_T=L_G^2\langle|\nabla T'|^2\rangle=2\pi^2L_G^2\overline{\sigma^2}, \tag{27}$$

with $\overline{\sigma^2}=\langle\sigma^2(t)\rangle_{\tau_p}$ and $\sigma^2(t)$ defined as in (19).

The Péclet number influences κ_T via two competing effects: on one hand, increasing Pe clearly enhances the mixing shear intensity given by $\mathrm{Pe}\,v(y)$, which should result in an increase in turbulent diffusivity. On the other hand, it also enhances the transverse sweep given by $\mathrm{Pe}\,w(t)$, this will be shown below to decrease the turbulent diffusivity. Theoretical predictions of the overall dependence of κ_T as a function of Pe as a result of this competition are given next. For the simplest case with $\beta=0$ in (3) so that $w(t)=w_0$ is a constant, one can derive an explicit expression for $\sigma^2(t)$ to be used in the expression for κ_T in (27). Otherwise, one can estimate $\sigma^2(t)$ asymptotically in the limit of large Péclet numbers; see Table I for a summary of the discussion below. Finally, an alternative would be to obtain $\sigma^2(t)$ numerically; this procedure is described at the end of this section.

A. Steady case $\beta=0$: Exact results

Detailed results in this case have been reported before[16]—they are summarized here to provide intuition for the unsteady case. With $w(t)=w_0$, the solution is steady with $\sigma^2(t)=\overline{\sigma^2}$ given explicitly by

$$\overline{\sigma^2}=\frac{\mathrm{Pe}^2/L_G^2}{4\pi^2(4\pi^2+\mathrm{Pe}^2\,w_0^2)}, \tag{28}$$

so that according to (27), the corresponding turbulent diffusivity is given by

TABLE I. Turbulent diffusivity with a deterministic steady single mode shear.

Cross-sweep $\mathrm{Pe}*[w_0+\beta\sin(\omega t)]$	Zeros in each period	Streamlines	Scaling κ_T
$0=\lvert\beta\rvert=\lvert w_0\rvert$	always	always open	Pe^2
$\lvert\beta\rvert=0<\lvert w_0\rvert$	never	always closed	Pe^0
$0<\lvert\beta\rvert<\lvert w_0\rvert$	none	always closed	Pe^0
$0<\lvert w_0\rvert<\lvert\beta\rvert$	two simple zeros	open twice per period	Pe^1
$0<\lvert w_0\rvert=\lvert\beta\rvert$	one double zero	open once per period	$\mathrm{Pe}^{4/3}$

$$\kappa_T=\frac{\mathrm{Pe}^2}{2(4\pi^2+\mathrm{Pe}^2\,w_0^2)}. \tag{29}$$

In conclusion, for a steady transverse sweep, we have the following.

(i) At small Pe: $\kappa_T\sim\mathrm{Pe}^2/8\pi^2$—the turbulent diffusivity is very small with a quadratic dependence on the Péclet number.
(ii) If $w_0=0$, i.e., in the absence of a transverse sweep: the same scaling $\kappa_T=\mathrm{Pe}^2/8\pi^2$ holds exactly for all values of Pe.
(iii) At large Pe with $w_0\neq 0$, i.e., with a steady nonzero transverse sweep: $\kappa_T\to 1/(2w_0^2)\sim\mathrm{Pe}^0$.

The sensitivity of κ_T to the intensity of the transverse shear via Pe has been explained[16] in terms of the topology of the streamlines: $w_0=0$ corresponds to open streamlines, transport by the shear parallel to the gradient is very effective while $w_0\neq 0$ corresponds to blocked streamlines, little distortion, and weak transport.

B. Unsteady case $\beta\neq 0$: Asymptotic results

Based on the discussion above for the steady transverse sweep, one would expect the following behavior in the unsteady transverse sweep case $w(t)=w_0+\beta\sin(\omega t)$ with β, $\omega\neq 0$. For small values of Pe, the transverse sweep is expected to have little impact on the solution. This will be confirmed in numerical experiments later in this section and could easily be verified asymptotically as a small perturbation of the zero transverse sweep case: as in the steady case, the turbulent diffusivity at small Pe is quadratic in Pe—we will not discuss this further. Instead, we focus on the behavior at large Pe. Most of the time, with $\beta\neq 0$, $w(t)$ is quite large at large Pe and streamline blocking should result in very limited turbulent mixing. However, should $w(t)$ vanish at some time t^*, streamlines would suddenly open with the potential for a tremendous boost in turbulent diffusivity. For such cases, the overall scaling of the turbulent diffusivity over a time period should be intermediate between the Pe^0 scaling from a constant nonzero transverse sweep and the Pe^2 scaling without a transverse sweep, with the precise exponent linked to the relative amount of time spent in the vicinity of the zeros for $w(t)$. Those intuitive considerations are confirmed next via large Péclet asymptotics. The single mode case $v(y)=\sin(2\pi y)$ corresponds to $\hat{v}_1=-i/2=-\hat{v}_{-1}$. Plugging in Duhamel's formula (11), (13):

$$\widehat{T_1'}=\frac{i}{2}\int_{-\infty}^{t}e^{-4\pi^2(t-t')}e^{-i2\pi\,\mathrm{Pe}\int_{t'}^{t}w(s)ds}, \tag{30}$$

with $\sigma^2(t)=2(\mathrm{Pe}^2/L_g^2)\lvert\widehat{T_1'}\rvert^2$. The expression for $\widehat{T_1'}$ is of the form $\int_{\infty}^{t}f(t')e^{i\,\mathrm{Pe}\,h(t')}dt'$. At large Péclet, the fast oscillations in the integrand cancel out for most of the time integration interval. The only potential contributions must come from stationary points $t'=t^*$ [i.e., points where $h(t')$ is extremum; in the present case, they correspond to the zeros of $w(t')$], where oscillations are much slower. If there are no stationary points, the next leading-order contribution comes from the end point $t'=t$, where cancellation is partial. Those ideas can be formalized via the stationary phase method (see, for example, Ref. 24) with the precise formula, depending essentially on the order of the zeros t^*. With a transverse sweep of the form $w(t)=w_0+\beta\sin\omega t$, $\beta\neq 0$, only three cases are possible as far as the order of the zeros are concerned.

(i) $0<\lvert\beta\rvert<\lvert w_0\rvert$: *the transverse sweep is always nonzero*. The main contribution to the quadrature comes from the end point. According to Ref. 24, $\sigma^2(t)$ is given to leading order by

$$\sigma^2(t)=\frac{1}{L_g^2}\frac{1}{4\pi^2[w_0+\beta\sin(\omega t)]^2}. \tag{31}$$

The turbulent diffusivity is computed using this expression in (27):

$$\kappa_T=\frac{\lvert w_0\rvert}{2\lvert w_0^2-\beta^2\rvert^{3/2}}. \tag{32}$$

This shows that, for cases where the transverse sweep never vanishes, the turbulent diffusivity at large Péclet behaves as in the constant nonzero transverse sweep case and saturates at a finite value.

(ii) $0\leqslant\lvert w_0\rvert<\lvert\beta\rvert$: *the transverse sweep has two simple zeros* in each period $t_{1,2}^*\in[0,\tau_P[$ defined by $\sin(\omega t^*)=-w_0/\beta$. According to the stationary phase method, the contribution from an order one zero is given to leading order by

$$\sigma^2(t)=\sigma_{\max}^2e^{-8\pi^2(t-t^*)},$$

with

$$\sigma_{\max}^2=\frac{\mathrm{Pe}\,\tau_P}{2\pi L_g^2\sqrt{\beta^2-w_0^2}}, \tag{33}$$

where $t>t^*$. Substituting this expression in (27) and summing over the two zeros gives the following expression for κ_T:

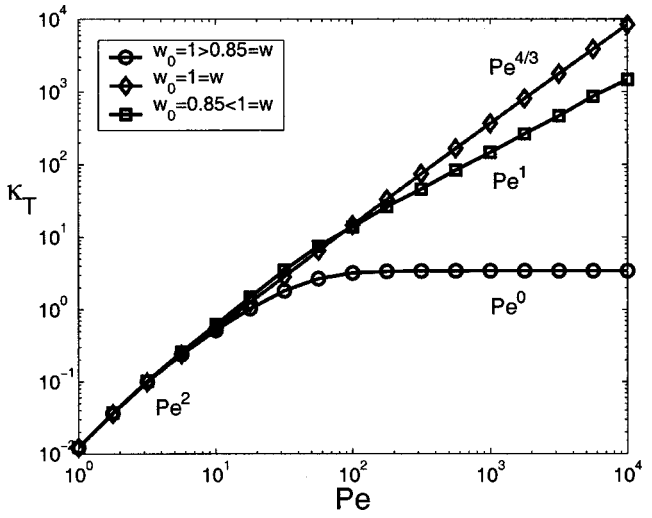

FIG. 2. Validation of scaling for κ_T.

$$\kappa_T = \frac{\mathrm{Pe}}{4\pi\sqrt{\beta^2 - w_0^2}}, \tag{34}$$

so that at large Péclet, $\kappa_T \sim \mathrm{Pe}$. This linear scaling, intermediate between the Pe^0 and Pe^2 with and without constant transverse sweep, is an indication of the tremendous contribution of the short time intervals where the streamlines open, allowing momentarily for intense mixing by the shear.

(iii) $0<|w_0|=|\beta|$: *the transverse sweep has one double zero* t^* *in* $[0,\tau_P[$ with either $t^*=0$ if β and w_0 have opposite signs or $t^*=\tau_P/2$ otherwise. Again, the main contribution to the quadrature comes from the stationary points. Applying the asymptotic formula to an order 2 stationary point[24] gives

$$\sigma^2(t) = \sigma^2_{\max} e^{-8\pi^2(t-t^*)}, \quad \text{with} \quad \sigma^2_{\max} = K^2 \frac{\mathrm{Pe}^{4/3}\,\tau_P^{4/3}}{\beta^{2/3} L_g^2}, \tag{35}$$

with the constant $K = 6^{1/3}\Gamma(1/3)/4\pi\sqrt{3}$. This leads to the following expression for κ_T:

$$\kappa_T = \frac{K^2}{4}\frac{\mathrm{Pe}^{4/3}\,\tau_P^{1/3}}{\beta^{2/3}}. \tag{36}$$

This time, $\kappa_T \sim \mathrm{Pe}^{4/3}$ grows superlinearly. The additional mixing compared to the case of two simple zeros can be explained by the fact that, in the present case, the flow spends a comparatively longer time in the vicinity of the zeros of the transverse speed, when most of the mixing occurs.

Remark: Both formulas (34) and (36) were derived, assuming that $\exp(-8\pi^2\tau_P)$ is negligible. If τ_P is not large enough for this to be the case, we will show that the stationary phase asymptotic strategy would not be valid anyway—see Sec. IV C.

C. Numerical validation

The predictions for the various scalings of κ_T as a function of Pe are summarized in Table I. For validation, we plot in Fig. 2, $\kappa_T(\mathrm{Pe})$ obtained by direct numerical computations for $\widehat{T_1'}$ using a numerical strategy described below. Results are shown for $1 \leqslant \mathrm{Pe} \leqslant 10^4$ for three cases representative of the three scaling regimes discussed above: the first case has $w_0 = 1 > 0.85 = \beta$ (no zero), the second case has $w_0 = 0.85 < 1 = \beta$ (two single zeros) and the third case has $w_0 = 1 = \beta$ (double zero). As expected, all three curves are very similar for very small Péclet, with a quadratic dependence. At large Péclet, the predicted scalings are verified, with, respectively, a horizontal asymptote, a linear scaling, and a superlinear scaling with exponent $\frac{4}{3}$.

The numerical strategy to compute $\sigma^2(t)$ directly, without any asymptotic approximation, is based on the following alternative formula[25] for the τ_P-periodic solution of the ODE in (12):

$$\widehat{T_J'}(t) = \widehat{T_*'}(t) - \widehat{T_*'}(\tau_P)[1 + S_{K_J}(t,0)]/S_{K_J}(\tau_P,0), \tag{37}$$

for $0 \leqslant t \leqslant \tau_P$, where $\widehat{T_*'}(t)$ is the solution of the same ODE (12), but with zero initial conditions instead of periodic conditions. In general, $\widehat{T_*'}(t)$ does not satisfy the periodicity condition. The formula in (37) exploits the linearity of the ODE to correct for periodicity. The numerical strategy based on (37) has two steps:

(i) Solve the initial value problem for $\widehat{T_*'}(t)$ using Matlab's fourth-order ODE integrator. At large Péclet, the ODE in (12) is not stiff for most parameters but has very fine time features that require time-step adaptivity for accuracy (see the discussion of the characteristic time scales in Sec. IV C).

(ii) Correct $\widehat{T_*'}$ according to (37). This is an explicit exact operation once $\widehat{T_*'}(\tau_P)$ has been computed in the first step.

The cost of computing $\widehat{T_J'}$ increases roughly linearly with Pe. For example, for the data in Fig. 2, it takes less than 1000 discrete time steps per period at low Péclet for four-digit accuracy on κ_T but up to a million discrete time steps per time period when $\mathrm{Pe} = 10^4$. Nevertheless, those ODE solutions remain extremely cheap (at most 30 min on a laptop with the full resolution of all scales for any data point in Fig. 2) compared to what it would take to solve the PDE in (1) if the spatial structure also had to be discretized.[25]

IV. SCALAR INTERMITTENCY FOR STEADY SINGLE MODE SHEARS

In the last section, the existence of isolated zeros in the transverse sweep has been linked to a mechanism for intermittent bursts of intense mixing that result in nontrivial Péclet scaling for the turbulent diffusivity. The same mechanism will now be shown to be associated with broader than Gaussian passive scalar PDFs. For simplicity in exposition, we restrict our study to the case of a transverse sweep of the form $w(t) = \beta \sin \omega t$, with $\beta > 0$, $\omega = 2\pi/\tau_P > 0$. This transverse sweep has exactly two single zeros in the period $[0,\tau_P[$: $t_1^* = 0$ and $t_2^* = \tau_P/2$ and the stationary phase approximation from (33) is directly applicable in the limit of

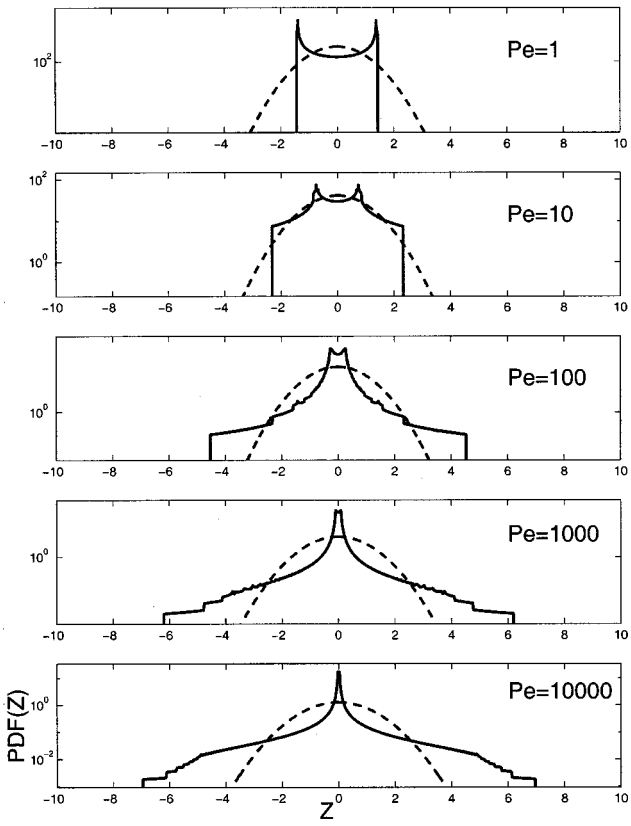

FIG. 3. The PDF as a function of Pe—deterministic single mode. Here and in similar plots below, the y axis is the usual logarithmic scale, $z=T'/\overline{\sigma}$, and the dashed line represents the Gaussian PDF with the same variance.

large Pe by simply setting $w_0=0$. Because of the symmetry in the two zeros t^*, the period of $\sigma^2(t)$ is now $\tau_P/2$, with $\sigma^2(t)$ given by

$$\sigma^2(t)=\sigma^2_{\max}e^{-8\pi^2 t}, \quad \text{with} \quad \sigma^2_{\max}=\frac{\mathrm{Pe}\,\tau_p}{2\pi L_g^2\beta}, \tag{38}$$

for $0\leqslant t\leqslant \tau_P/2$. This expression will now be used in the general formulas (21), (23) to derive explicit asymptotic expressions at large Péclet numbers for the PDF of the passive scalar in the case of a steady single mode shear with, respectively, a deterministic or a stationary Gaussian random amplitude. Examples of PDFs obtained using numerical computations of $\sigma^2(t)$ are also reported.

A. PDFs for a deterministic steady single mode shear

1. Numerical results: Transition from sub-Gaussian to broad-tail PDFs

Figure 3 shows the results of numerical experiments with $\beta=1$, Pe=1, 10, 100, 1000, 10 000, $\tau_P=0.5$, and the deterministic steady single mode shear $v(y)=\sin(2\pi y)$ (also discussed in Sec. II B). The PDFs were obtained by the discrete quadrature of (21) with $\sigma^2(t)$ computed numerically following the strategy outlined in Sec. III. Also shown as dashed lines are the Gaussian PDFs with the same variance. When Pe=1, the PDF displays the typical double-peak sine PDF in (20), which is clearly sub-Gaussian. As the Péclet number increases, however, the double-peak core shrinks, the normalized fluctuations become larger, with the PDFs tails clearly becoming progressively broader.

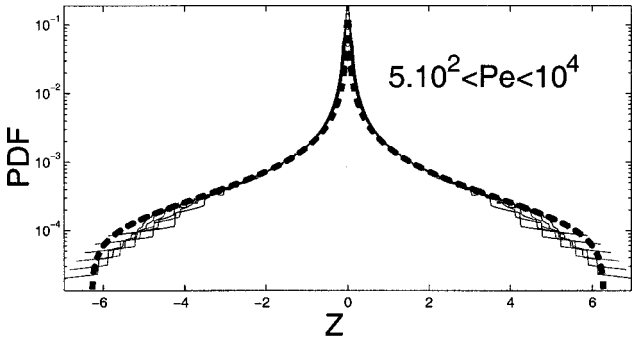

FIG. 4. Asymptotic PDF (dashed line) shape for a deterministic single mode compared to the numerical results for a range of large Péclet numbers (solid lines).

2. Asymptotic limiting shape

In Fig. 4, the PDFs for eight values of Pe in the range $500<\mathrm{Pe}<10\,000$ are superimposed to demonstrate the existence of a limiting shape. This limiting shape is predicted asymptotically, by integrating exactly the general formula in (21) with $\sigma^2(t)$ given at large Péclet by (38) to yield the following.

Self-similar PDF for the deterministic case. In the limit of large Pe,

$$p(T')=\frac{1}{\overline{\sigma}}p_\infty\left(\frac{T'}{\overline{\sigma}}\right), \tag{39}$$

with

$$p_\infty(z)=K_1\frac{\pi-2\arcsin(K_2|z|)}{K_2|z|}, \tag{40}$$

where K_1 is a normalizing constant and $K_2=1/\sqrt{4\pi^2\tau_P}$.

This expression is valid for $\sigma_{\min}<|T'|<\sigma_{\max}$ with $\sigma_{\min}=\sigma_{\max}\exp(-2\pi^2\tau_P)$ the very small size of the inner core. This asymptotic PDF shape is shown in Fig. 4 as a thick dashed line. The agreement for moderately large values of the normalized fluctuations $|T'|/\overline{\sigma}$ is excellent. As Pe increases, the agreement extends to increasingly large values of $|T'|/\overline{\sigma}$ as the asymptotic stationary phase approximation for $\sigma^2(t)$ used to obtain (40) becomes more relevant.

B. PDFs for a stationary Gaussian random shear

1. Numerical results: Transition from Gaussian to broad-tail PDFs

Using the same data for $\sigma^2(t)$ as above, numerical PDFs based on (23) are generated that correspond to the case of a shear with steady stationary Gaussian random amplitude. Figure 5 displays the PDFs with increasing Péclet numbers, along with the Gaussian PDFs with the same variance. At Pe=1, the PDF is Gaussian. At Pe=10, there still appears to be a Gaussian core, but its support has shrunk, the tails are broader, and the PDF resembles an exponential distribution.

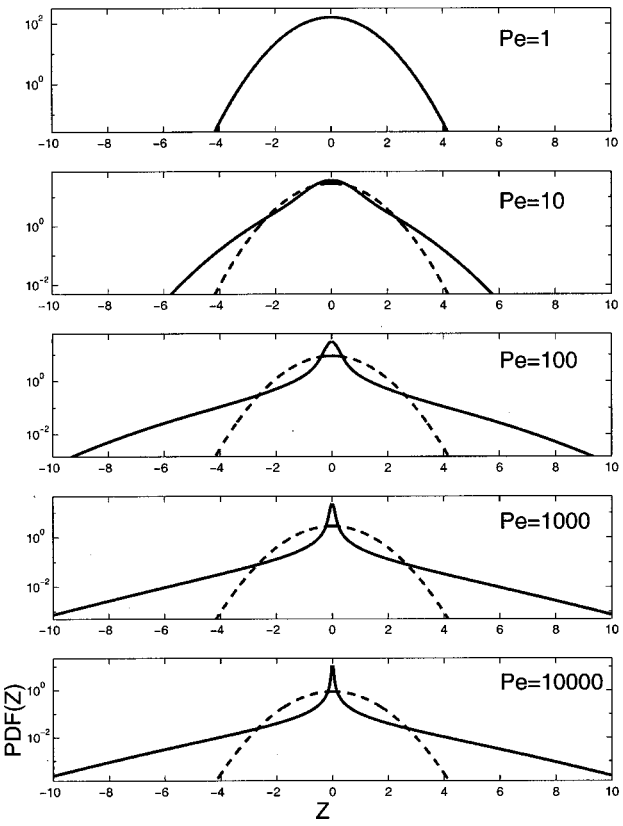

FIG. 5. The same as in Fig. 3 for the case of a random stationary Gaussian single mode.

This trend continues for Pe=100 and larger, the PDF has even broader tails with an overall shape closer to a stretched exponential distribution.

2. Asymptotic limiting shape

As for the deterministic case in Sec. IV A, the PDFs converge at large Péclet to a universal limiting shape that can be predicted asymptotically by integrating exactly (23) with the asymptotic approximation for $\sigma^2(t)$ in (38).

3. Self-similar PDF for the steady stationary Gaussian random case

In the limit of large Pe,

$$p(T') = \frac{1}{\overline{\sigma}} p_\infty\left(\frac{T'}{\overline{\sigma}}\right), \tag{41}$$

with

$$p_\infty(z) = K_1 \frac{\mathrm{erf}(CK_2 z) - \mathrm{erf}(K_2 z)}{K_2 z}, \tag{42}$$

where K_1 is a normalizing constant, $K_2 = 1/\sqrt{4\pi^2\tau_P}$, and $C = \exp(2\pi^2\tau_P)$ is a very large constant.

This formula is valid for $|z|$ outside the inner core. This asymptotic shape is shown in Fig. 6 along with the PDFs for eight values of Pe in the range $500 < \mathrm{Pe} < 10\,000$ with excellent agreement.

Remark: The range $|T'| < 10\overline{\sigma}$ in Figs. 5 and 6 was selected because it corresponds to a representative range for reliable experimental data or numerical data with more complex models. In the present formulation, accurate numerical or asymptotic values could be generated quite easily, even for arbitrarily rare events. The trend observed for large values of $|T'|/\overline{\sigma}$ is similar to the one observed in Fig. 4: the PDF drops markedly since there can be no significant contributions at very large values. The regime that appears to follow a stretched exponential applies only for a finite band extending over many standard deviations of the Gaussian.

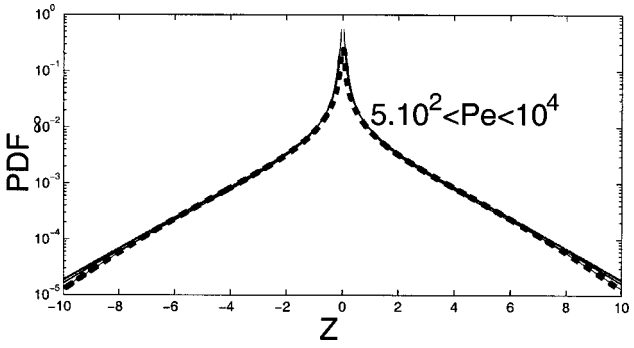

FIG. 6. The same as in Fig. 4 for the case of a random stationary Gaussian single mode.

To summarize, the transition depicted in Fig. 5 from Gaussian PDF to exponential PDF (around Pe=10) to a universal stretched exponential PDF (for Pe>100) is therefore qualitatively similar to experimental results as well as numerical results obtained with more complex models, at least for a reasonable range of values. The asymptotic explicit formula in (42), however, indicates that the limiting shape cannot be described everywhere by the stretched exponential that one typically obtains by a best fit based on a limited range of values over a few standard deviations of the Gaussian. Such limited range fits are what is actually used in processing experimental or numerical data.

C. Asymptotic regimes

To conclude this section, we will now address the following issue. We have just documented the existence of self-similar PDFs with strong intermittency in the limit of large Péclet numbers as a result of a bursting mechanism linked to isolated zeros in the transverse sweep. In the experiments above, good agreement between the numerical PDFs at large but finite Péclet and the asymptotic self-similar PDF occurred, beginning at values on the order of Pe~100.

In general, how large should the Péclet number be for strong intermittency?

We will answer this question by stating more precisely the conditions on Pe in relation to the other parameters in the model that need to be satisfied for the self-similar intermittent regime to exist. With $w(t) = \beta \sin(\omega t)$, the model (11), (13) becomes

$$T'(y,t) = \frac{\mathrm{Pe}}{L_g}(\widehat{T'_J} e^{iK_J y} + \text{c.c.}),$$

with

$$\frac{d\widehat{T_J'}}{dt}+[K_J^2+iK_J\,\mathrm{Pe}\,\beta\sin(\omega t)]\widehat{T_J'}=-\widehat{v_J}. \tag{43}$$

Rescaling the length by $1/K_J$ and the time by $1/K_J^2$ leads to a convenient formulation that does not depend explicitly on K_J:

$$T'(y,t)=\frac{\mathrm{Pe}'}{L_g'}(\widehat{T_J'}e^{iy}+\text{c.c.}),$$

with

$$\frac{d\widehat{T_J'}}{dt}+[1+i\,\mathrm{Pe}'\,\beta\sin(\omega' t)]\widehat{T_J'}=-\widehat{v_J}, \tag{44}$$

through the rescaled variables $K_J y\to y$, $K_J^2 t\to t$, $\mathrm{Pe}'=\mathrm{Pe}/K_J$, $L_g'=L_gK_J$, and $\omega'=2\pi/\tau_P'=\omega/K_J^2$. In all the computations in this section, it will be assumed that the energy of the shear has been normalized so that $|E_J|=2|\widehat{v_J'}|^2=1$. To analyze the behavior of the solution for $\widehat{T_J'}$, we identify the following four characteristic time scales in (44):

- viscous relaxation time, $\tau_v'=1$;
- flow forcing period, $\tau_P'=2\pi/\omega'$;
- fast sweep time, $\tau_{\mathrm{fs}}'=1/(\mathrm{Pe}'\,\beta)$;
- slow sweep time $\tau_{\mathrm{ss}}'=\sqrt{\tau_P'/(\mathrm{Pe}'\,\beta)}$.

The viscous relaxation time τ_v' is unity here because of the choice of characteristic length and time scales above. The forcing time scale τ_P' is self-explanatory. As described in the Introduction, the transverse sweep affects the topology of the streamlines, with important consequences regarding the turbulent diffusivity. The topology of the streamlines is an Eulerian view of the physics of the problem; as far as extracting a time scale, a Lagrangian view provides in the present case a more useful diagnostic: the effect of the transverse sweep is measured in terms of the time it takes a particle to sweep vertically across the shear's period due to advection. This sweep time concept remains valid even when the transverse sweep is modulated in time, at least for Péclet numbers sufficiently large, with the only difference that the sweep time will also be modulated in time in that case. When the transverse sweep intensity is maximum, the sweep time reaches its minimum value, called from now on the *fast sweep time scale*; little turbulent diffusion is expected for values of the sweep time in the neighborhood of the fast sweep time. At the zero-crossing of the transverse sweep, however, the sweep time reaches its maximum value, called from now on the *slow sweep time scale*; it is associated with bursts of intense turbulent mixing. Explicit formulas for the fast and slow sweep times are derived by first introducing the expression for the characteristic sweep time $\tau_{\mathrm{sweep}}'(t_0)$ around an arbitrary time t_0 in the period. It is given implicitly by

$$\int_{t_0}^{t_0+\tau_{\mathrm{sweep}}'(t_0)}\mathrm{Pe}'|w(t)|dt=1.$$

With $w(t)=\beta\sin 2\pi t/\tau_P'$, this formula becomes

$$\mathrm{Pe}'\,\beta\left|\cos\left(\frac{2\pi t_0}{\tau_P'}\right)-\cos\left(\frac{2\pi(t_0+\tau_{\mathrm{sweep}}')}{\tau_P'}\right)\right|=\frac{2\pi}{\tau_P'}. \tag{45}$$

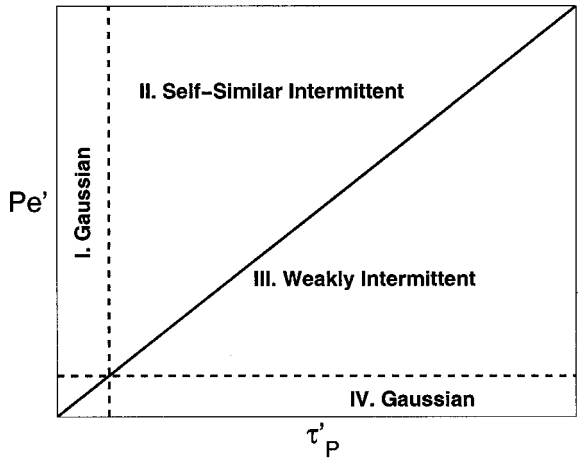

FIG. 7. Phase diagram (Pe', τ_P') of the asymptotic regimes; steady case.

This definition makes sense only when $\mathrm{Pe}'\,\beta$ is sufficiently large for a solution for τ_{sweep}' to exist; we will get back to this condition later. The quantity $\tau_{\mathrm{sweep}}'(t_0)$ takes on a range of values for $0<t_0<\tau_P'/2$ with the fastest time τ_{fs}' corresponding to $t_0=\tau_P'/4$ when $w(t)$ is maximum and the slowest time corresponding to $t_0=0$ when $w(t_0)=0$. The formulas for τ_{fs}' and τ_{ss}' are obtained by Taylor expansion of the general expression for τ_{sweep}' in (45) at these locations.

Previously, we have explained the intermittent behavior as a result of a burst of intense mixing by the shear when the transverse sweep is zero compared to very little mixing when the transverse sweep is large. In terms of the time scales we have just identified, it is clear that this mechanism is relevant only if the following order is respected:

$$\tau_{\mathrm{fs}}'\ll\tau_{\mathrm{ss}}'\ll\tau_P'. \tag{46}$$

With the formulas for the time scales above, this condition is equivalent to $\mathrm{Pe}'\,\beta\tau_P'$ being sufficiently large; we will come back to this condition later on in the discussion. There are four ways to order $\tau_v'=1$ in (46); next, we show that each order corresponds to a regime characterized by a definite type of PDF and mixing intensity:

- Regime I: $\tau_{\mathrm{fs}}'<\tau_{\mathrm{ss}}'<\tau_P'<\tau_v'=1$;
- Regime II: $\tau_{\mathrm{fs}}'<\tau_{\mathrm{ss}}'<\tau_v'=1<\tau_P'$;
- Regime III: $\tau_{\mathrm{fs}}'<\tau_v'=1<\tau_{\mathrm{ss}}'<\tau_P'$;
- Regime IV: $\tau_v'=1<\tau_{\mathrm{fs}}'<\tau_{\mathrm{ss}}'<\tau_P'$.

Figure 7 shows a phase diagram with the boundary of each regime in terms of Pe' and τ_P'. Next, a detailed description is developed where we identify for each regime the appropriate asymptotic strategy to derive an explicit expression for $\sigma^2(t)$. This expression is then used to characterize each regime via two representative scalar quantities that are very easily computed.

(i) The turbulent diffusivity, $\kappa_T=L_g'^2\overline{\sigma^2}$.
(ii) The intermittency ratio R_{σ^2} defined as $\sigma^2_{\max}/\overline{\sigma^2}$. In the present setup, the ratio R_{σ^2} is a very good indicator of

the intermittency and the behavior of the tails of the PDFs; it is extremely easy to compute with an explicit formula for $\sigma^2(t)$. Because of its definition, $R_{\sigma^2} \geqslant 1$. Values close to one correspond to Gaussian PDF; large values indicate broad tails and a large departure from Gaussianity.

At the end of this section, we confirm the predictions developed below through numerical quadrature of the solution.

1. Regime I: $\tau'_P < \tau'_v = 1$

In regime I, viscous effects are very slow. Viscosity is the main mechanism by which the solution adjusts to the forcing, including the adjustment to the effect of the transverse sweep. Hence, in regime I, the viscous time is too long for the solution to respond significantly to the perturbations due to the transverse sweep, small or large, because those perturbations occur on much shorter time scales. A rigorous treatment of this regime can be found in Appendix B of Ref. 25. The solution is built as a series expansion in terms of the small parameter τ'_P. The zeroth-order term is shown to be time independent. Solvability for the first-order term leads to the condition that the leading-order term is the steady solution without the transverse sweep. It is trivial to solve (44) for $\widehat{T'_J}(t)$ and compute $\sigma^2(t)$:

$$|\widehat{T'_J}|^2 = E_J/2 = 1/2, \quad \sigma^2(t) = \frac{\mathrm{Pe}'^2}{L_g'^2} = \sigma^2_{\max} = \overline{\sigma^2}. \tag{47}$$

Using this expression in the formula for κ_T and R_{σ^2}:

$$\text{Regime I} \quad \kappa_T = \mathrm{Pe}'^2, \quad R_{\sigma^2} = 1.$$

This last value indicates that the PDF in regime I is Gaussian.

2. Regime II: $\tau'_{ss} < \tau'_v < \tau'_P$

This corresponds to the condition that $1 < \tau'_P < \mathrm{Pe}'\,\beta$. During most of the time period, streamlines are blocked, and the amplitude $\sigma(t)$ is small. During the short slow sweep time interval, however, streamlines are open and the solution grows very rapidly. Because $\tau'_{ss} < \tau'_v$, this growth is basically inviscid and $\sigma(t)$ increases until the streamlines become blocked again, at the end of the slow sweep time interval. At that point, $\sigma(t)$ will tend to decrease back to a much smaller value, with the decay controlled exclusively by molecular viscosity. This dynamics of an inviscid burst followed by a viscous relaxation phase is precisely captured by the stationary phase asymptotic approximation that was utilized earlier in this section. Formula (38) for $\sigma^2(t)$ can be used directly; the value for $\sigma_{\max}$ can be linked very precisely to the inviscid growth phase, followed by the viscosity controlled exponential decay. Processing the explicit expression for $\sigma^2(t)$ from (38) leads to

$$\text{Regime II} \quad \kappa_T = \frac{\mathrm{Pe}'}{\beta}, \quad R_{\sigma^2} = \tau'_P.$$

Here are some remarks regarding regime II.

(i) The intermittency ratio $R_{\sigma^2} = \tau'_P$ is large, away from the boundary with regime I to the left. This indicates strong intermittency, along with the fact that $\kappa_T \sim \mathrm{Pe}'$ can become arbitrarily large at large Pe.

(ii) Also, R_{σ^2} is independent of Pe′. This indicates self-similar intermittency at fixed τ'_P.

3. Regime III: $\tau'_{fs} < \tau'_v < \tau'_{ss}$

This corresponds to the condition that $1 < \mathrm{Pe}'\,\beta < \tau'_P$. In that regime, large fluctuations in the scalar are still associated with the neighborhood of the stationary points, due to streamline blocking away from those points, as in regime II. However, on the time scale of the slow sweep time interval, the role of viscosity is much more significant than it was in regime II. Therefore, a good asymptotic approximation is that viscous relaxation forces the solution to adjust fully to the forcing while the transverse sweep is slow. This is the quasisteady approximation: instantaneous adjustment is assumed. Strictly speaking, it is not quite valid for the entire time period, because the effect of streamline blocking associated with the fast sweep time still occur on a very fast time scale compared to the viscous time. However, this turns out to make little difference as long as the dominant contribution from the slow sweep time interval is well captured. Setting the time derivative to zero in (44), one can solve explicitly for $\widehat{T'_J}(t)$ and compute $\sigma^2(t)$:

$$\sigma^2(t) = \frac{\mathrm{Pe}'^2}{L_g'^2} \frac{1}{1 + \mathrm{Pe}'^2\,\beta^2 \sin(2\pi t/\tau'_P)^2}.$$

Notice that this is very different from the steady solution in regime I, where the solution is completely steady because the transverse sweep is ignored altogether. In the present regime, the transverse sweep plays a big role and the solution is very timedependent. The maximum instantaneous variance is $\sigma^2_{\max} = \mathrm{Pe}'^2/L_g'^2$ and the average variance over a time period is $\overline{\sigma^2} = \mathrm{Pe}'^2/(L_g'^2\sqrt{1+\mathrm{Pe}'^2\,\beta^2})$. This leads to

$$\text{Regime III} \quad \kappa_T = \frac{\mathrm{Pe}'^2}{\sqrt{1+\mathrm{Pe}'^2\,\beta^2}}, \quad R_{\sigma^2} = \sqrt{1+\mathrm{Pe}'^2\,\beta^2}.$$

Here are some remarks regarding Regime III.

(i) Here κ_T and R_{σ^2} are independent of τ'_P. This is consistent with the quasisteady asymptotic approach.

(ii) Here κ_T and R_{σ^2} both increase as a function of Pe′, starting from near-Gaussian values when $\mathrm{Pe}\,\beta \sim 1$ until the exit into regime II when $\mathrm{Pe}'\,\beta \sim \tau'_P$, where maximum intermittency is achieved at a given value of τ'_P.

4. Regime IV: $\tau'_v < \tau'_{fs}$

This corresponds to the condition that $\mathrm{Pe}'\,\beta < 1$. If Pe′ is decreased further, so that τ'_v becomes smaller than any other time scale in the system, in particular, smaller than the fast sweep time, then the quasisteady approximation used in regime III becomes rigorously applicable at all times; also see the discussion in Ref. 25. The results for κ_T and R_{σ^2} in

TABLE II. Asymptotic regimes for the steady single mode case.

Regime	Time scales order	κ_T	$R_{\sigma^2}=\sigma^2_{\max}/\overline{\sigma^2}$
I Gaussian (steady)	$\tau'_P<\tau'_v$ $(\tau_P K_J^2<1)$	$\dfrac{\mathrm{Pe}^2}{K_J^2}$	1
II Self-similar intermittent (stationary phase)	$\tau'_{ss}<\tau'_v<\tau'_P$ $(1<\tau_P K_J^2<\mathrm{Pe}\,\beta/K_J)$	$\dfrac{\mathrm{Pe}}{K_J\beta}$	$\tau_P K_J^2$
III Transition weakly intermittent (quasisteady)	$\tau'_{fs}<\tau'_v<\tau'_{ss}$ $(1<\mathrm{Pe}\,\beta/K_J<\tau_P K_J^2)$	$\dfrac{\mathrm{Pe}^2}{K_J\sqrt{K_J^2+\mathrm{Pe}^2\,\beta^2}}$	$\sqrt{1+\dfrac{\mathrm{Pe}^2\,\beta^2}{K_J^2}}$
IV Gaussian (regular limit III)	$\tau'_v<\tau'_{fs}$ $(\mathrm{Pe}\,\beta/K_J<1)$	$\dfrac{\mathrm{Pe}^2}{K_J^2}$	1

regime IV can therefore be obtained directly by taking the regular limit of $\mathrm{Pe}'\,\beta$ very small in the expressions in Regime III:

Regime IV $\quad \kappa_T=\mathrm{Pe}'^2, \quad R_{\sigma^2}=1.$

The PDF reduces to a Gaussian distribution, unlike in regime I, however, absolute fluctuations are asymptotically small since $\kappa_T\sim\mathrm{Pe}'^2$ is very small in this regime. With $\mathrm{Pe}'\,\beta$ so small, the whole transverse sweep time concept is questionable anyway, as the equation (45) no longer has a solution that defines $\tau'_{\mathrm{sweep}}(t_0)$ at any t_0 in the time period.

Remark: It is easy to verify that the condition in (46) is automatically satisfied in regimes II and III, the only two regimes where intermittency is possible, so that (46) does not constitute an additional constraint for intermittency.

The formulas applicable in each regime are summarized in Table II, where the explicit dependence with K_J has been reintroduced. Next, the PDF regimes in Table II are confirmed through numerical quadrature.

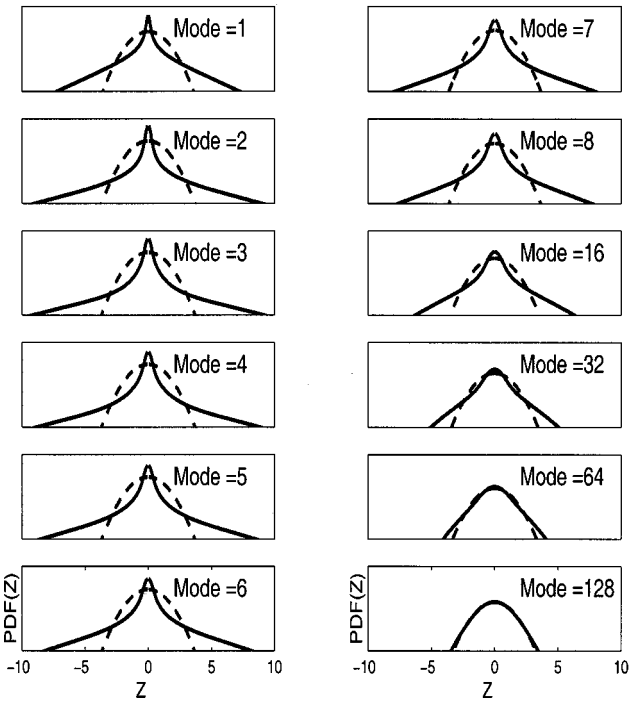

FIG. 8. The PDFs corresponding to mode numbers J with $K_J=2\pi\{1,2,3,...\}$.

As a first validation, we reinterpret the series of PDFs reported in Fig. 5. The parameters in those experiments are $\tau_P=0.5$, $K_J=2\pi$, and $\beta=1$. This gives $\tau'_P=K_J^2\tau_P=19\gg1$, larger than the critical value below which the PDF is always Gaussian at all Péclet numbers. Increasing Pe at constant K_J and τ_P corresponds to a vertical trajectory in the phase diagram: $\mathrm{Pe}=1$ corresponds to $\mathrm{Pe}'\,\beta=0.16<1$, regime IV, the range $10<\mathrm{Pe}<100$ correspond to regime III and $\mathrm{Pe}>100$ to regime II. The monotone increase in non-Gaussianity until a self-similar PDF is reached as observed in Fig. 6 is consistent with the predictions for R_{σ^2} in regimes II and III.

A second set of PDFs is presented in Fig. 8. In these experiments, $\mathrm{Pe}=1000$, $\tau_P=0.5$ and $\beta=1$ are fixed, but K_J is varied with $K_J=2\pi\{1,2,3,4,5,6,7,8,16,32,64,128\}$. This corresponds to a trajectory in phase space described by $\tau'_P=0.5K_J^2$ and $\mathrm{Pe}'=1000/K_J$. The different test cases can be roughly classified as follows: modes 1–2–3 are in regime II, modes 4 to 64 are in regime III, and mode 128 is in regime IV. The numerical results are in excellent agreement with the predicted behavior in each regime.

(i) Going from mode 1 to mode 3, the PDFs become broader as K_J increases. This is consistent with the expression for $R_{\sigma^2}=\tau_P K_J^2$ in regime II.
(ii) Once in regime III (modes 4 to 64), the PDFs become

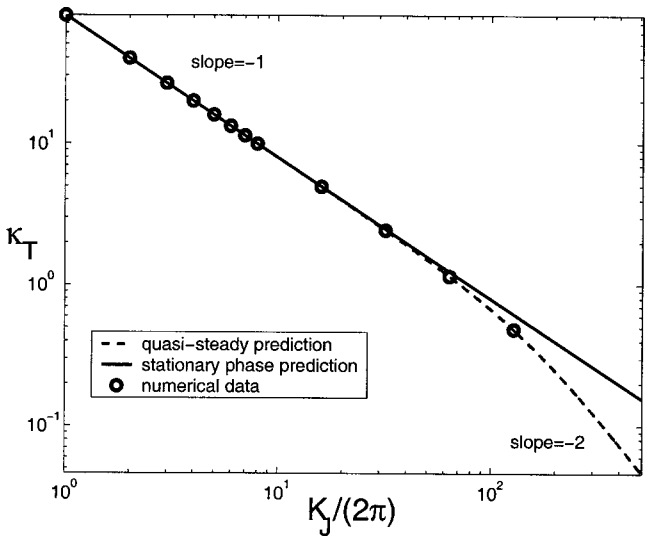

FIG. 9. Turbulent diffusivity corresponding to Fig. 7.

narrower as K_J is increased further, in good agreement with the prediction that $R_{\sigma^2}=\sqrt{1+\mathrm{Pe}^2\,\beta^2/K_J^2}$ in regime III.

(iii) Finally, at mode 128, the PDF is Gaussian, as predicted in regime IV.

Figure 9 shows κ_T corresponding to all those cases. Again, excellent agreement with the theoretical predictions is observed, with a K_J^{-1} dependence at small K_J both in regime II and regime III, and, ultimately, a K_J^{-2} dependence at large K_J in regimes III and IV.

We conclude this discussion by answering the question formulated at the beginning of this section. The interesting self-similar intermittent regime identified previously, with very large turbulent diffusivity and large fluctuations in the scalar (on an absolute scale) corresponds to regime II, the regime where stationary phase asymptotics is appropriate. Besides the existence of isolated zeros in the transverse sweep, the analysis in terms of time scales has identified two additional conditions for intermittent bursts to occur and lead to an interesting scalar PDF.

Condition 1: The slow sweep time must be shorter than the viscous time. This guarantees that the sudden amplification in the scalar response linked to the streamlines opening when the transverse sweep is very small occurs on a time scale short enough not to be hampered by molecular viscosity. This condition is always satisfied in the limit of very large Pe. If condition 1 is not satisfied, then the system is in the quasisteady asymptotic regime. It is possible that the PDFs still display broad tails with large normalized fluctuations, but on an absolute scale, fluctuations and the turbulent diffusivity are small, so that the system would be characterized as weakly intermittent.

Condition 2: The forcing period must be long compared to the viscous time. Condition 2 guarantees that the transverse sweep will have a noticeable effect on the solution. If condition 2 is not satisfied, then oscillations are too fast for the transverse sweep to be effective and the bursting mechanism associated with the modulation in transverse sweep does not apply, no matter how large the Péclet number—very strong mixing can be observed, but the PDFs are necessarily Gaussian.

V. SCALAR INTERMITTENCY FOR RANDOM SPATIOTEMPORAL AND MULTIMODE SHEARS

Unlike the steady singlemode shears analyzed so far, real turbulent flows usually have energy spectra with a wide range of space and time scales. Here scalar intermittency is studied in the elementary models when the shear flow $v(y,t)$ is a spatiotemporal Gaussian random field to mimic some of these effects. In Sec. V A we describe the effect of unsteadiness via a finite correlation time while in Sec. V B the effect of the distribution of the shear energy over several modes is studied. The objective is to identify the conditions where self-similar strongly intermittent PDFs, as analyzed for the steady single mode case can be observed with more complex spatiotemporal flows. The template of asymptotic regimes developed in Sec. IV C for the steady case will be very useful here to guide the possible regimes of behavior for the scalar PDF in the present situation.

A. Random spatiotemporal single mode shears

Here we consider unsteady stationary Gaussian random flows, with a single mode K_J and the temporal behavior at that mode characterized by a correlation time τ_J, such that

$$R_J(|t|)=E_J e^{-|t|/\tau_J}, \tag{48}$$

with $R_J(|t|)$ the covariance introduced in (25) and E_J the shear energy at mode K_J. The formulas to be given below are for $E_J=1$. This introduces the new time scale τ_J in the problem, in addition, to the four time scales previously identified in the steady case. First we show that, to a large extent, the effect of this new time scale can be understood in terms of the steady shear problem by considering a reduced viscous relaxation time scale $\tau_{v,\mathrm{unsteady}}=\tau_{v,\mathrm{steady}}/[1+1/(\tau_J K_J^2)]$. One important consequence of this observation is that one recovers the expected Gaussian PDFs in the limit of δ-correlated shear flows. Indeed, with the expression for the reduced viscous relaxation time above, the limit $\tau_J\to 0$ is equivalent to the limit of very short effective viscous relaxation times, which correspond to regime IV in the steady case, with Gaussian PDFs. The asymptotic analysis to justify this result is given next, along with a discussion of the other asymptotic regimes. All these predictions are validated by numerical simulations to be found at the end of this section.

The first step in the analysis is to rescale the equations. With the covariance of the form (48), Duhamel's formula (13) generalizes to

$$\sigma^2(t)=\frac{\mathrm{Pe}^2}{L_g^2}\int_{-\infty}^{t}\int_{-\infty}^{t} S_{K_J}(t,t')S_{K_J}(t,\tilde{t})R_J(|t'-\tilde{t}|)\,dt'\,d\tilde{t}. \tag{49}$$

It is an exercise for the reader to check from (49) that when $R_J(|t|)$ is a delta function, $\sigma^2(t)$ is constant, and the PDF is Gaussian. A more practical formulation is derived in the appendix, where it is shown that $\sigma^2(t)$ can be computed alternatively as

$$\sigma^2(t)=\frac{\mathrm{Pe}^2}{L_g^2}[I^2(t)+D(t)],$$

where $I^2(t)=|\widehat{T_J'}|^2$, with $\widehat{T_J'}$ the periodic solution of the following equation:

$$\frac{d\widehat{T_J'}(t)}{dt}+[K_J^2+1/\tau_J+iK_J\,\mathrm{Pe}\,\beta\sin(\omega t)]\widehat{T_J'}=\widehat{v_J'}, \tag{50}$$

while $D(t)$ is the periodic solution of

$$\frac{dD(t)}{dt}+2K_J^2D-\frac{2}{\tau_J}I^2=0. \tag{51}$$

The complex ODE in (50) is identical to the ODE from (15) used in the steady case, except that the viscous coefficient K_J^2 in (15) has been replaced here by the enhanced coefficient K_J^2+1/τ_J. This suggests we rescale time and length in (50) with $T=1/(K_J^2+1/\tau_J)$ and $L=1/K_J$. This rescaling leads to

TABLE III. Asymptotic regimes for the single mode case with correlation time τ_J'.

Regime	$\sigma^2_{\max}$	κ_T	$R_{\sigma^2}=\sigma^2_{\max}/\overline{\sigma^2}$
I Gaussian	$\dfrac{\mathrm{Pe}^2}{L_g^2K_J^2(K_J^2+1/\tau_J)}$	$\dfrac{\mathrm{Pe}^2}{K_J^2+1/\tau_J}$	1
II Self-similar intermittent	$\dfrac{\mathrm{Pe}\,\tau_P}{L_g^2\beta K_J}$	$\dfrac{\mathrm{Pe}}{\beta K_J}$	$\tau_P K_J^2$
III Weakly intermittent	$\dfrac{\mathrm{Pe}^2}{L_g^2K_J^2(K_J^2+1/\tau_J)}$	$\dfrac{\mathrm{Pe}^2}{\sqrt{(K_J^2+1/\tau_J)^2+K_J^2\,\mathrm{Pe}^2\,\beta^2}}$	$\sqrt{1+\dfrac{K_J^2\,\mathrm{Pe}^2\,\beta^2}{(K_J^2+1/\tau_J)^2}}$
IV Gaussian	$\dfrac{\mathrm{Pe}^2}{L_g^2K_J^2(K_J^2+1/\tau_J)}$	$\dfrac{\mathrm{Pe}^2}{K_J^2+1/\tau_J}$	1

$$\frac{d\widehat{T_J'}(t)}{dt}+[1+i\,\mathrm{Pe}''\,\beta\sin(\omega''t)]\widehat{T_J'}=\widehat{v_J'},$$
$$\sigma^2(t)=\frac{\mathrm{Pe}''^2}{L_g'^2}(I^2+D), \tag{52}$$

with $I^2(t)$ and $D(t)$ defined as above, provided that $\mathrm{Pe}''=\mathrm{Pe}'/(1+1/\tau_J')$, $\omega''=\omega'/(1+1/\tau_J')$, with $\tau_J'=\tau_J K_J^2$ and $\mathrm{Pe}'=\mathrm{Pe}/K_J$, $\omega'=\omega/K_J^2$, $L_g'=L_gK_J$ as in the steady case. The rescaled equation (52) is now identical to the rescaled steady-case version in (44) analyzed in Sec. IV C so that the numerical and asymptotic strategies used previously in the steady case can be generalized in a very straightforward fashion to obtain the solution to (52). The second part of the problem is to compute the correction $D(t)$ according to the equation (51). This is a linear equation with constant coefficients that is trivial to solve, numerically or asymptotically, once the forcing term $I^2(t)$ is known. A systematic asymptotic analysis is summarized below. First we describe the key results with a phase diagram and with Table III that generalizes the steady-case results in Table II.

1. Phase diagram (Fig. 10)

In the unsteady case with correlation time τ_J', the same regimes that were identified in Sec. IV C for the steady case exist and are defined by the same constraints on the parameters as those in Table II as long as everything is rescaled according to the reduced viscous relaxation time, $\tau_v=1/(K_J^2+1/\tau_J)$, i.e., Pe'' replaces Pe'; τ_P'' replaces τ_P'.

(i) Regime I, $\tau_P''<1$;
(ii) regime II, $\tau_{ss}''<1<\tau_P''$;
(iii) regime III, $\tau_{fs}''<1<\tau_{ss}''$;
(iv) regime IV, $1<\tau_{fs}''$;

where $\tau_{fs}''=1/(\mathrm{Pe}''\,\beta)$ and $\tau_{ss}''=\sqrt{\tau_P''\tau_{fs}''}$ similar to the expression for the steady case. The phase diagram in Fig. 10 shows the boundaries of the regimes in terms of $\mathrm{Pe}'=\mathrm{Pe}/K_J$ and $1/\tau_J'=1/(\tau_J K_J^2)$ for fixed values of $\tau_P'=\tau_P K_J^2$ and β. This diagram applies whenever $\tau_P'>1$. Because $\tau_P''>\tau_P'>1$ for all values of τ_J', it is clear that the solution in the present case never belongs to regime I, even in the steady limit with $1/\tau_J'\to 0$. The effect of a finite correlation time can be understood by considering, for example, a value of Pe' sufficiently large that the self-similar intermittent regime is observed in the steady case, i.e., the solution belongs to regime II when $1/\tau_J'=0$. According to the diagram (see also Table III and the asymptotic analysis that follows), one can see that decreasing the correlation time (increasing $1/\tau_J'$) will correspond to decreasing intermittency with a transition from regime II to regime III, and ultimately to regime IV and Gaussian PDFs. This is the expected behavior in the limit of δ-correlated shears; this limit is valid regardless of the Péclet number whenever the correlation time is shorter than any other time scale in the problem, including the fast sweep time. Numerical results that confirm the scenario just described are given at the end of this section.

There are many qualitative similarities between this phase diagram and the one presented in Ref. 12, Fig. 2, where three regimes for the PDFs (Gaussian, exponential, stretched exponential) are identified through processing direct numerical simulations of a more complex random field model. The PDFs that we observe in each regime roughly correspond to the same classification as in Ref. 12, with Gaussian PDFs in regime IV, exponential PDFs in regime III, and stretched exponentials in regime II (see, however, the comments in Sec. IV B regarding the range of data typically used for fitting such a specific distribution).

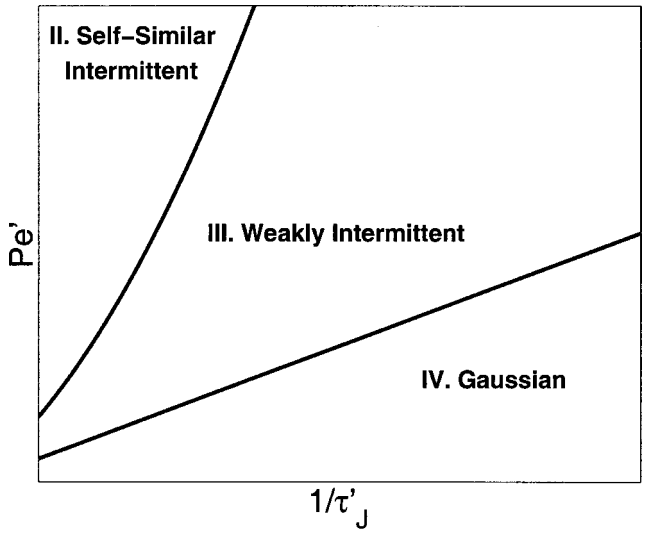

FIG. 10. Phase diagram (Pe', $1/\tau_J'$) of the asymptotic regimes; unsteady random case.

2. Solution in each regime (Table III)

Table III generalizes the formulas from Table II to the unsteady case with correlation time τ'_J. Again, to prepare for the multimode analysis, the explicit dependence with respect to K_J has been reintroduced. The derivations in each regime are very similar to the corresponding steady case, so few details are given here.

(i) Regime I. The steady approximation applies to $I^2(t)$ via the solution of (52). This implies necessarily that $D(t)$ is also a constant that does not depend on time and so does $\sigma^2(t)=I^2+D$:

$$\sigma^2=(1+1/\tau'_J)\frac{\mathrm{Pe}''^2}{L'^2_g}.$$

Notice that this regime is observed only when $\tau_P<1/(K_J^2+1/\tau_J)$, hence a necessary condition is that $\tau_P<\tau_J$, i.e., that the correlation time be long compared to the forcing period.

(ii) Regime II. The stationary phase is used for $I^2(t)$, the asymptotic expression for $I^2(t)$ is simple, and $D(t)$ can be found exactly, with the result that $\sigma^2(t)=I^2(t)+D(t)$ does not depend on $1/\tau'_J$, even though both $I^2(t)$ and $D(t)$ do. The explicit formula for $\sigma^2(t)$ in regime II turns out to remain unchanged compared to the expression in (38) for the steady case, and, as a consequence, so are the formula for κ_T, etc. for regime II, Table III. An intuitive explanation of this somewhat unexpected result is as follows. As in the steady case, the dynamics of the solution in regime II is characterized by two important phases. The first phase occurs during the slow sweep time interval during which horizontal transport by the shear is very intense with $\sigma^2(t)$ growing to its maximum value in a time too short for either molecular viscosity or the finite correlation time of the shear to have any effect. The second phase follows: as soon as streamlines are blocked again, outside the slow sweep time interval, the shear becomes ineffective at distorting the scalar and $\sigma^2(t)$ will tend to drop back to relatively small values. What controls the decay is molecular viscosity only, as in the steady case. In particular, the finite correlation time of the shear can play no role in this decay because the effect of the shear has been blocked altogether by the transverse sweep. Numerical results reported at the end of this section confirm this prediction.

(iii) Regime III. The quasisteady approximation can be used to solve for $I^2(t)$. It can also be used to solve for $D(t)$ only if $\tau'_P>1$. We will restrict our study to cases where this condition is satisfied, in which case one has the following formula for $\sigma^2(t)$:

$$\sigma^2(t)=(1+1/\tau'_J)\frac{\mathrm{Pe}''^2}{L'^2_g}\frac{1}{1+\mathrm{Pe}''^2\,\beta^2\sin(\omega''t)^2}.$$

(iv) Regime IV. As in the steady case, this is simply the limit for Pe″ very small compared to 1 in the expressions for regime III.

The asymptotic predictions are verified in Fig. 11 and Fig. 12 with a series of computations for decreasing correlation times τ_J. Here, $K_J=2\pi$, Pe=1000, $\tau_P=0.5$, and $\beta=1$ while $1/\tau'_J=1/(\tau_J K_J^2)=0$, 1/4, 1/2, 1, 2, 4, 8, 16, 32, 64, 128, 256. With those data, we expect the following asymptotic regimes: the range $0<1/\tau'_J<4$ corresponds to regime II, the range $4<1/\tau'_J<100$ to regime III, and $100<1/\tau'_J$ to regime IV. There is very good agreement between the asymptotic predictions in each regime and the numerical experiments. For instance, in Fig. 11, there is basically no impact of τ'_J on the PDFs corresponding to regime II cases, as predicted in Table III and discussed above. For shorter correlation times (as $1/\tau'_J$ increases), a progressive narrowing of the PDFs occurs as the system moves through regime III, reducing finally

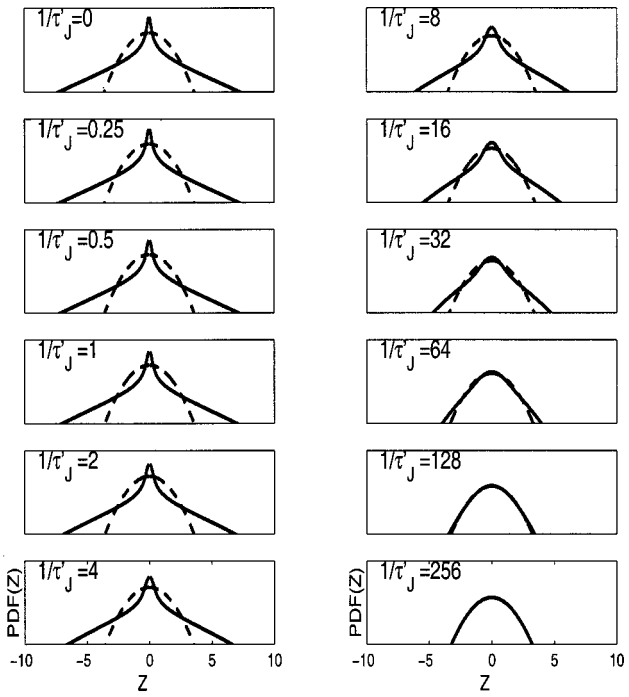

FIG. 11. The PDFs corresponding to various correlation times τ'_J. Note that the second column resembles the exponential to Gaussian transition often documented elsewhere (Refs. 3 and 12).

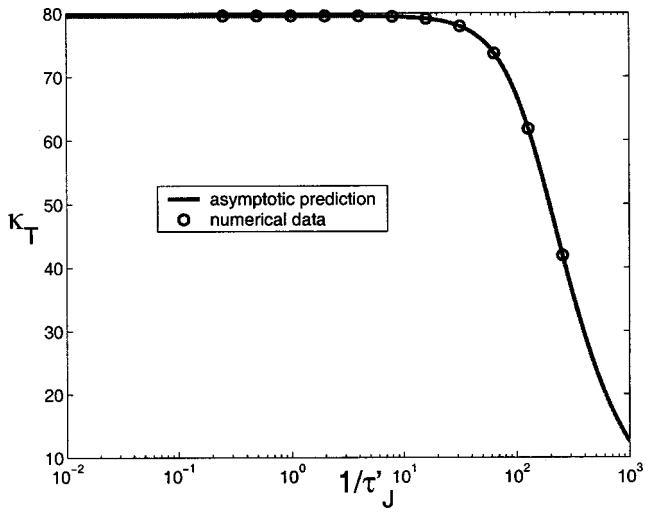

FIG. 12. Turbulent diffusivity corresponding to Fig. 11.

to a Gaussian PDF, as expected in the limit of a δ-correlated shear ($1/\tau_J'$ very large). Similar conclusions can be drawn from Fig. 12. reducing the correlation time has no effect on the turbulent diffusivity at large correlation times, but has a much more significant impact with a marked reduction in κ_T for very short correlation time τ_J.

B. Random spatiotemporal multimode shears

According to the predictions in Table III, it is clear that either increasing the wave number K_J or decreasing the correlation time τ_J always leads eventually to less intermittent PDFs because the effective viscous relaxation time scale $1/(K_J^2+1/\tau_J)$ decreases. One could therefore wonder if the strongly intermittent behavior that we have identified in this paper could be observed in cases where the shear has a more realistic energy spectrum with multiple spatiotemporal modes, including many with high mode numbers and short correlation times. In this section, we demonstrate that this is the case if the most energetic mode individually belongs to the self-similar strongly intermittent regime. The analysis is carried out by assuming an energy spectrum of the form

$$E_J \propto K_J^{-\alpha}, \tag{53}$$

for modes $K_J=2\pi\{1,2,...,N\}$. Typical choices for α are $\alpha=1$ (Batchelor) or $\alpha=\frac{5}{3}$ (Kolmogorov). The correlation time of each mode is also expressed by a power law, with large values of K_J corresponding to shorter correlation times:

$$\tau_J=\tau_C K_J^{-\alpha'}, \tag{54}$$

with $\tau_C>0$ the correlation time constant. Again, typical choices for α' are $\alpha'=1$ (eddy sweeping time) or $\alpha'=\frac{2}{3}$ (Kolmogorov Lagrangian decorrelation time).[16]

Based on the results in Table III, next we predict the scaling with K_J for the multimode case. Assume a spectrum of N modes with $K_J=2\pi J$, $J=1,2,...,N$ and total energy Pe^2. The energy fraction in mode J is given by $E_J=K_J^{-\alpha}/\Sigma K_J^{-\alpha}$. We will consider test cases where mode 1 ($K_1=2\pi$) belongs to regime II, so that if the energy is concentrated in that mode, the self-similar strongly intermittent behavior is observed. To address the question of the impact of spreading the shear energy over a larger number of modes, we use the values in Table III with the scalings in (53), (54) to predict the overall dependence on K_J of the higher modes. With mode 1 belonging to regime II, higher modes belong necessarily to either regime II, regime III, or regime IV, but never to regime I.

(i) Contribution from a mode in regime II:
$\sigma^2_{\max}\sim K_J^{-(1+\alpha)}$; $\sigma^2\sim K_J^{-(3+\alpha)}$; $\kappa_T\sim K_J^{-(1+\alpha)}$.

(ii) Contribution from a mode in regime III:
$\sigma^2_{\max}\sim K_J^{-(4+\alpha)}$; $\sigma^2\sim K_J^{-(3+\alpha)}$; $\kappa_T\sim K_J^{-(1+\alpha)}$.

(iii) Contribution from a mode in regime IV:
$\sigma^2_{\max}\sim K_J^{-(4+\alpha)}$; $\sigma^2\sim K_J^{-(4+\alpha)}$; $\kappa_T\sim K_J^{-(2+\alpha)}$.

The conclusions from this analysis are as follows.

(i) Higher modes will contribute little to the far tails of the intermittent PDFs because the maximum range to which they contribute, as measured by $\sigma^2_{\max}$, decreases like $K_J^{-1-\alpha}$ (in regime II) or even faster in regimes III and IV. They will contribute even less to the bulk of the PDF because their contribution, in terms of $\overline{\sigma^2}$, decreases even faster. As a result, no noticeable change in the overall shape of the PDF of the most energetic mode is to be expected when the energy is spread among many modes.

(ii) With $\alpha'<2$, the effect of the correlation time compared to the effect of the molecular viscosity diminishes as the mode number increases: therefore, the correlation time τ_J is expected to have no impact on the solution at very high modes, even if it can have a significant impact at low modes.

(iii) The turbulent diffusivity will include contributions of order $K_J^{-1-\alpha}$ from all modes K_J, up to the cutoff in regime IV, where contributions decrease much faster and are negligible. Summing over all modes gives the approximation

$$\frac{\kappa_{T,N}}{\kappa_{T,1}}=\frac{\Sigma K_J^{-1-\alpha}}{\Sigma K_J^{-\alpha}}, \tag{55}$$

where $\kappa_{T,i}$ is the turbulent diffusivity with an energy spectrum that includes i modes.

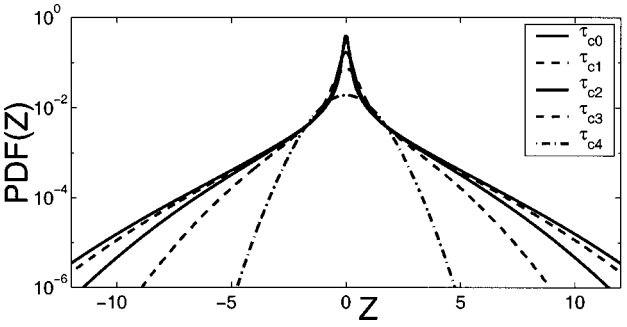

FIG. 13. The PDFs corresponding to various τ_J and the number of modes in the energy spectrum, $\alpha=1$.

These predictions are validated in Figs. 13 and 14 for the

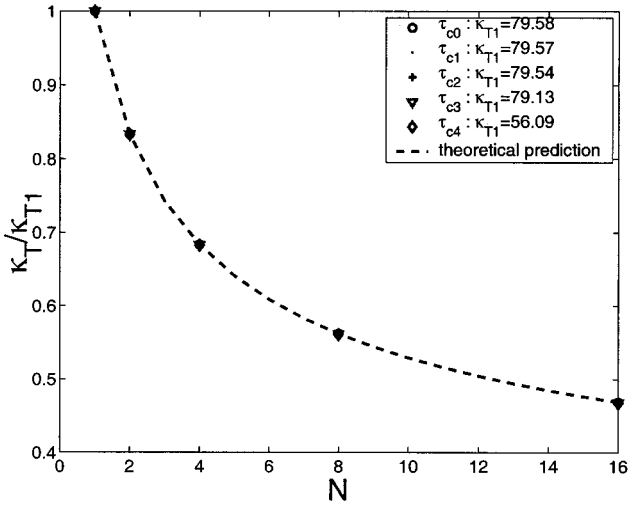

FIG. 14. (Scaled) turbulent diffusivity corresponding to Fig. 13.

spectral exponents $\alpha=\alpha'=1$, similar results (not reported here) are obtained with the other choices of exponents in (53), (54). Five combinations of modes were considered: (1) just one mode $K_1=2\pi$; (2) two modes K_1, K_2; (3) four modes K_1, K_2, K_3, K_4; (4) eight modes from K_1 up to K_8; (5) 16 modes from K_1 up to K_{16}. Five choices for the correlation time parameter τ_C are also considered: $1/\tau_{C0}=0$, $1/\tau_{C1}=2\pi$, $1/\tau_{C2}=8\pi$, $1/\tau_{C3}=32\pi$, $1/\tau_{C4}=1000$ (the first set with $1/\tau_{C0}=0$ corresponds to steady cases already shown in Fig. 11). All 25 PDFs are superimposed in Fig. 13. The most striking feature is that it is impossible to distinguish between the different mode combinations for a given value of the correlation-time constant τ_C; this is in agreement with the predictions that the presence of higher modes should not affect the overall shape of the PDF. The other observation is that decreasing the correlation time constant τ_C results in a transition from a broad tail PDF when $1/\tau_C=0$ to a Gaussian PDF for $1/\tau_C=1000$; this effect was discussed at length in Sec. V A in the case of a single mode shear. Figure 14 shows the turbulent diffusivity corresponding to those cases. The values of κ_T for a given combination of modes are renormalized by κ_{T1} corresponding to the single mode, with the same correlation time constant. While κ_{T1} was seen in Fig. 12 to vary substantially with $1/\tau_C$, the fact that all five sets of data collapse onto one curve in Fig. 14 confirms that the rescaled quantity κ_{TN}/κ_{T1} depends only on the number of modes included, not on the correlation time constant. Agreement with the crude approximation in (55), shown as a dashed line, is excellent.

VI. CONCLUDING DISCUSSION

An elementary model has been introduced in this paper and utilized to establish scalar intermittency in PDFs with an imposed large-scale gradient in an unambiguous fashion through elementary analytical techniques and numerical quadrature of exact formulas. The PDF shapes that emerge in the regime of intermittency resemble those that have been documented from post-processing of numerical solutions of much more complex models.[12,13] Analytical theory has been utilized to successfully predict the asymptotic shape of the PDFs for $\mathrm{Pe}\gg 1$. The simplest examples from Sec. IV involving steady deterministic or random single mode shears with a time-dependent transverse sweep prove that neither positive Lyapunov exponents for the particle trajectories nor a multimode turbulent spectrum are needed to generate scalar intermittency. What these models have is a mechanism where there is an intermittent burst in time of strong transport parallel to the mean gradient due to a change in streamline structure. As documented in Secs. III and IV, this effect conspires with molecular diffusivity to produce the intermittent PDFs at larger Péclet numbers. The results in Sec. V for random spatiotemporal shears, showing a decrease in scalar intermittency as the decorrelation time τ_J tends to zero for a fixed large Péclet number, also provide unambiguous theoretical predictions and supporting evidence in a simple model for such behavior, which has been documented earlier in more complex simulations (see Fig. 2 of Ref. 12). It would be interesting to investigate scalar intermittency for generalizations of the model with a random transverse sweep and with a multiscale turbulent inertial range for the shear flow.[16] In the present paper we focus on scalar PDFs for the elementary model introduced in (1), (2), (4). Other interesting statistics of the scalar such as the conditional dissipation and PDFs for scalar increments in y can be calculated in a similar fashion and will be presented elsewhere by the authors in the near future. All these statistics are important in testing closure strategies for nonpremixed turbulent combustion[26–29] in an unambiguous fashion and the present models are very useful in that context.[26] It would be interesting to check the structure of the PDFs at large Péclet numbers for scalar intermittency for the wide variety of space–time periodic flows, where homogenization theory is valid.[16]

ACKNOWLEDGMENTS

The research of A.B. is partially supported by a grant from NSERC and by ARO under Grant No. DAAG55-98-1-0129. The research of A.J.M. is partially supported by the ARO under Grant No. DAAG55-98-1-0129, by the ONR under Grant No. N00014-96-1-0043, and by the National Science Foundation under Grant No. DMS-9972865.

APPENDIX: FORMULATION FOR THE RANDOM SPATIOTEMPORAL CASE

Duhamel's formula (49) for $\sigma^2(t)$ in the unsteady case is of the form

$$I=\int_{\tilde{t}=-\infty}^{\tilde{t}=t}\int_{t'=-\infty}^{t'=t} S_{-K_J}(t,t')S_{K_J}(t,\tilde{t})R_j(|t'-\tilde{t}|)dt'd\tilde{t}, \tag{A1}$$

with

$$S_{K_J}(t,t')=\exp\left(-K_J^2(t-t')-iK_J\,\mathrm{Pe}\int_{t'}^{t}w(s)ds\right), \tag{A2}$$

with $w(t)=\beta\sin\omega t$ the transverse shear. Split the integral into two parts:

$$I=I_1+I_2, \tag{A3}$$

where I_1 corresponds the half of the domain, where $\tilde{t}>t'$, I_2 the other half. First, we develop a strategy to compute I_1. For I_1, one has

$$R_j(|t'-\tilde{t}|)=R_j(\tilde{t}-t'). \tag{A4}$$

Therefore

$$I_1=\int_{\tilde{t}=-\infty}^{\tilde{t}=t} e^{-2K_J^2(t-\tilde{t})} \times\int_{t'=-\infty}^{t'=\tilde{t}} e^{-K_J^2(\tilde{t}-t')}e^{iK_J\,\mathrm{Pe}\int_{t'}^{\tilde{t}}w(s)ds}R_j(\tilde{t}-t')dt'd\tilde{t}, \tag{A5}$$

$$=\int_{\tilde{t}=-\infty}^{\tilde{t}=t} e^{-2K_J^2(t-\tilde{t})}J_1(\tilde{t})d\tilde{t}, \tag{A6}$$

where

$$J_1(\tilde{t}) = \int_{t'=-\infty}^{t'=\tilde{t}} e^{-K_J^2(\tilde{t}-t')} e^{iK_J \,\mathrm{Pe} \int_{t'}^{\tilde{t}} w(s)ds} R_j(\tilde{t}-t')dt', \tag{A7}$$

with the important remark that $J_1(\tilde{t})$ is independent of t itself. Both $J_1(\tilde{t})$ and $I_1(t)$ are periodic functions of their argument with period τ_v from the velocity forcing.

If one assumes the following special form for the correlation function:

$$R_j(\tilde{t}-t') = e^{-(\tilde{t}-t')/\tau_J}. \tag{A8}$$

Then the expression for $J_1(\tilde{t})$ becomes

$$J_1(\tilde{t}) = \int_{t'=-\infty}^{t'=\tilde{t}} e^{-(K_J^2+1/\tau_J)(\tilde{t}-t')} e^{iK_J \,\mathrm{Pe} \int_{t'}^{\tilde{t}} w(s)ds} dt'. \tag{A9}$$

Both $I_1(t)$ and $J_1(\tilde{t})$ can be computed as solutions of the following ODEs:

$$\frac{dJ_1(\tilde{t})}{d\tilde{t}} = 1 - \left(K_J^2 + \frac{1}{\tau_J} - iK_J \,\mathrm{Pe}\, w(\tilde{t}) \right) J_1(\tilde{t}), \tag{A10}$$

$$\frac{dI_1(t)}{dt} = J_1(t) - 2K_J^2 I_1(t). \tag{A11}$$

Similarly,

$$\frac{dJ_2(\tilde{t})}{d\tilde{t}} = 1 - \left(K_J^2 + \frac{1}{\tau_J} + iK_J \,\mathrm{Pe}\, w(\tilde{t}) J_2(\tilde{t}) \right), \tag{A12}$$

$$\frac{dI_2(t)}{dt} = J_2(t) - 2K_J^2 I_2(t). \tag{A13}$$

It is easy to verify that $I_2(t) = \overline{I_1}(t)$ and $J_2(t) = \overline{J_1}(t)$. One can then easily derive the ODEs satisfied by $|J(t)|^2 = J_1(t)J_2(t)$ and by $I(t) = I_1(t) + I_2(t)$:

$$\begin{aligned} \frac{d|J|^2}{dt} &= J_1(t) + J_2(t) - 2(K_J^2 + 1/\tau_J)|J|^2, \\ \frac{dI}{dt} &= J_1(t) + J_2(t) - 2(K_J^2) I. \end{aligned} \tag{A14}$$

Define $I(t) = |J(t)|^2 + D(t)$. Then the difference $D(t)$ satisfies

$$\frac{dD}{dt} = -2K_J^2 D(t) + \frac{2}{\tau_J}|J|^2. \tag{A15}$$

For the special case with $1/\tau_J = 0$, it is clear that the only periodic solution of this last equation is $D(t) = 0$. Hence, $D(t)$ can be viewed as a finite correlation time correction to $|J|^2$ to get the variance $I = \sigma^2(t)$.

[1] B. Castaing, G. Gunaratne, F. Heslot, L. Kadanoff, A. Libchaber, S. Thomae, X. Wu, S. Zaleski, and G. Zanetti, "Scaling of hard thermal turbulence in Rayleigh–Bénard convection," J. Fluid Mech. **204**, 1 (1989).

[2] F. Heslot, B. Castaing, and A. Libchaber, "Transition to turbulence in helium gas," Phys. Rev. A **36**, 5870 (1987).

[3] J. P. Gollub, J. Clarke, M. Gharib, B. Lane, and O. N. Mesquita, "Fluctuations and transport in a stirred fluid with a mean gradient," Phys. Rev. Lett. **67**, 3507 (1991).

[4] B. R. Lane, O. N. Mesquita, S. R. Meyers, and J. P. Gollub, "Probability distributions and thermal transport in a turbulent grid flow," Phys. Fluids A **5**, 2255 (1993).

[5] Jayesh and Z. Warhaft, "Probability distribution of a passive scalar in grid-generated turbulence," Phys. Rev. Lett. **67**, 3503 (1991).

[6] Jayesh and Z. Warhaft, "Probability distribution, conditional dissipation, and transport of passive temperature fluctuations in grid-generated turbulence," Phys. Fluids A **4**, 2292 (1992).

[7] A. R. Kerstein, "Linear-eddy modelling of turbulent transport. Part 6. Microstructure of diffusive scalar mixing fields," J. Fluid Mech. **231**, 361 (1991).

[8] A. Pumir, B. Shraiman, and E. D. Siggia, "Exponential tails and random advection," Phys. Rev. Lett. **66**, 2984 (1991).

[9] M. Holzer and A. Pumir, "Simple models of non-Gaussian statistics for a turbulently advected passive scalar," Phys. Rev. E **47**, 202 (1993).

[10] A. R. Kerstein and P. A. McMurtry, "Mean-field theories of random advection," Phys. Rev. E **49**, 474 (1994).

[11] M. Chertkov, G. Falkovich, I. Kolokolov, and V. Lebedev, "Statistics of a passive scalar advected by a large-scale two-dimensional velocity field: Analytic solution," Phys. Rev. E **51**, 5609 (1995).

[12] E. S. C. Ching and Y. Tu, "Passive scalar fluctuations with and without a mean gradient: A numerical study," Phys. Rev. E **49**, 1278 (1994).

[13] K. Ngan and R. T. Pierrehumbert, "Spatially correlated and inhomogeneous random advection," Phys. Fluids **12**, 822 (2000).

[14] R. T. Pierrehumbert, "Lattice models of advection–diffusion," Chaos **10**, 61 (2000).

[15] M. Holzer and E. D. Siggia, "Turbulent mixing of a passive scalar," Phys. Fluids **6**, 1820 (1994).

[16] A. J. Majda and P. R. Kramer, "Simplified models for turbulent diffusion: Theory, numerical modelling, and physical phenomena," Phys. Rep. **314**, 237 (1999).

[17] A. J. Majda, "The random uniform shear layer: An explicit example of turbulent diffusion with broad tail probability distributions," Phys. Fluids A **5**, 1963 (1993).

[18] R. M. McLaughlin and A. J. Majda, "An explicit example with non-Gaussian probability distribution for nontrivial scalar mean and fluctuation," Phys. Fluids **8**, 536 (1996).

[19] J. C. Bronski and R. M. McLaughlin, "The problem of moments and the Majda model for scalar intermittency," Phys. Lett. A **265**, 257 (2000).

[20] J. C. Bronski and R. M. McLaughlin, "Rigorous estimates of the tails of the probability distribution function for the random linear shear model," J. Stat. Phys. **98**, 897 (2000).

[21] E. Vanden Eijnden, "Non-Gaussian invariant measures for the Majda model of decaying turbulent transport," Commun. Pure Applied Math. (to appear).

[22] A. Bensoussan, J. L. Lions, and G. Papanicolaou, "Asymptotic analysis for periodic structures," Number 5 in *Studies in Mathematics and its Applications* (North Holland-Elsevier, Amsterdam, 1978).

[23] A. M. Yaglom, *Correlation Theory of Stationary and Related Random Functions. Volume I: Basic Results* (Springer-Verlag, Berlin, 1987).

[24] A. H. Nayfeh, *Introduction to Perturbation Techniques* (Wiley, New York, 1981), pp. 80–86.

[25] J. Bonn and R. M. McLaughlin, "Sensitive enhanced diffusivities for flows with fluctuating mean winds: a two-parameter study," J. Fluid Mech. **445**, 345 (2001).

[26] A. Bourlioux and A. J. Majda, "An elementary model for the validation of flamelet approximations in non-premixed turbulent combustion," Combust. Theory Modell. **4**, 189 (2000).

[27] A. W. Cook and J. J. Riley, "Subgrid-scale modeling for turbulent reacting flows," Combust. Flame **112**, 593 (1998).

[28] J. Jimenez, A. Linan, M. M. Rogers, and F. J. Higuera, "*A priori* testing of subgrid models for chemically reacting non-premixed turbulent shear flows," J. Fluid Mech. **349**, 149 (1998).

[29] A. D. Leonard and J. C. Hill, "Scalar dissipation and mixing in turbulent reacting flows," Phys. Fluids A **3**, 1286 (1991).